Improvement of affinity and potency of a monoclonal antibody against *Shigella flexneri* 3a O-antigen via phage display and whole-cell in-solution panning

Nicholas L. Xerri[1], Sophia Pulido[1], Mateusz Kędzior[1], Paul Savarino[1], Torrey Williams[1], Robert M. Gallant[1], Robert W. Kaminski[2], Devin Sok[3], Hayden R. Schmidt[1*]

[1] IAVI Neutralizing Antibody Center, San Diego, California, USA

[2] Latham Biopharm Group, Cambridge, Massachusetts, USA

[3] Global Health Investment Corporation, New York, New York, USA

[*]Correspondance: hschmidt@iavi.org

Abstract:
As rates of antimicrobial resistance (AMR) among bacterial pathogens continue to rise, the discovery and development of novel classes of therapeutics that can serve as alternatives or adjuncts to traditional small-molecule antibiotics, such as monoclonal antibodies (mAbs), is a public health priority. Some of the most promising antigen targets for antibacterial mAbs are surface polysaccharides such as O-antigen, a component of the lipopolysaccharide found on the outer membrane of gram-negative bacteria. However, developing mAbs against bacterial surface polysaccharides with sufficient breadth and potency to be clinically viable is difficult in part because antibodies against polysaccharides are generally low affinity, and the challenging biochemistry of polysaccharides often precludes further affinity maturation of mAbs against these targets *in vitro*. Here, we use a phage display library and a whole-cell in-solution panning strategy to successfully improve the affinity of a mAb against *Shigella flexneri* 3a O-antigen (O-Ag) *in vitro* without requiring the purification of the target antigen. We demonstrate that a single mutation can improve apparent affinity approximately 10-fold without detectably increasing polyreactivity, and increased affinity correlates with enhanced potency in antibacterial effector function and anti-virulence assays. In addition, the most potent variants also gained increased breadth, successfully coordinating complement deposition and complement-independent opsonophagocytosis against *S. flexneri* 3b, a serotype weakly recognized by the parent mAb. Altogether, this work represents an important first step towards expanding the antibody engineering toolkit for bacterial surface polysaccharides, which will aid the development of novel mAb therapeutics against AMR bacterial pathogens.

Author Summary:
Monoclonal antibodies are a type of therapeutic that hold promise for the treatment of infections cause by antibiotic-resistant bacteria. The best antibody targets on bacteria are often complex sugars (called polysaccharides) on the bacterial surface. Unfortunately, antibodies against these sugars usually bind their targets weakly, meaning they are not potent enough to be effective therapies. Improving these antibodies in the laboratory is difficult, because polysaccharide biochemistry is challenging. In this paper, we use a novel strategy to improve the potency of an antibody against a bacterial polysaccharide

without needing to chemically isolate the polysaccharide. We create a library of antibody mutants that we display on bacterial viruses called phage, and then mix these phages with whole bacterial cells. After washing the mixture, we can knock the phage off the cells and use DNA sequencing to measure which mutants stuck best (and specifically) to the target bacterium. Using this approach, we found mutations in our antibody that help it bind the target polysaccharide better, and we show that this improvement leads to more broad and potent antibacterial effects *in vitro*. Altogether, this fast and easy approach may be used to develop better antibody therapeutics against bacterial pathogens.

Introduction:

Antimicrobial resistance (AMR) among pathogenic bacteria is a rapidly growing threat that necessitates the development of novel therapeutics to supplement existing antibiotics(1). Monoclonal antibodies (mAbs) may be complementary to antibiotics because they can prevent and treat AMR infections by both recruiting effector cells to kill bacteria via Fc-mediated effector functions (i.e., complement-driven bactericidal activity or complement independent opsonophagocytosis), and by directly interfering with bacterial virulence(2). Some of the most promising antigens for antibacterial immunotherapies are polysaccharides on the bacterial surface. Surface polysaccharides are well validated targets for approved bacterial vaccines (e.g., those against *Haemophilus influenzae* b, *Streptococcus pneumoniae*, *Neisseria meningitidis*, and *Salmonella typhi*) (3–7). This provides a strong rationale for developing anti-polysaccharide mAbs, and anti-polysaccharide mAbs against several bacterial species have been shown to be effective in preclinical animal models (8–17). However, to date, few of these mAbs against bacterial polysaccharides have been evaluated in clinical trials. Panobacumab, an IgM mAb against O-antigen (O-Ag) from serotype O11 *Pseudomonas aeruginosa* obtained promising results in a phase IIa trial among patients with pneumonia, though the effect size was modest and no control arm was present (18), so additional studies are required to fully assess clinical benefit. Gremubamab, a bispecific mAb targeting the exopolysaccharide PsI and the protein PcrV, has entered the clinic (19) and recently shown promise in treating *P. aeruginosa* infections in patients with bronchiectasis, though similarly, this was a proof-of-concept trial and more studies are required to ensure reproducible clinical efficacy (20).

One reason for the small number of both clinical trials and anti-polysaccharide mAb candidates in the pipeline is that discovering and engineering anti-polysaccharide mAbs that have sufficient breadth and potency to be clinically viable is challenging. Breadth for a given anti-polysaccharide mAb is often too narrow for clinical use because the chemical structures of most surface polysaccharides are highly variable (even within the same bacterial species (21). Bacterial strains of a given species are typically grouped into serotypes (often dozens or more) based on the specific chemical structure of key surface polysaccharides (such as the O-Ag, which is a component of gram-negative lipopolysaccharide), and antibody responses against these bacteria are usually serotype-specific (22,23). In addition to breadth, potency is another challenge for anti-polysaccharide mAbs since B cells targeting repetitive polysaccharide antigens undergo T cell independent responses that generate short-lived plasma antibody responses, which are predominately IgM with minimal somatic mutation and low affinity for the target

antigen (24). While there are examples of high affinity anti-bacterial polysaccharide mAbs that have undergone extensive affinity maturation isolated from the peripheral blood mononuclear cells of convalescent donors (16), it is unclear how widespread this phenomenon is. In principle, additional high-potency mAbs against bacterial surface polysaccharides can be developed by engineering high-affinity variants of known anti-bacterial polysaccharide mAbs through *in vitro* affinity maturation. The chemical heterogeneity, inherent complexity of polysaccharide biochemistry, and the conformational flexibility of these polysaccharides (leading to a high entropic cost for binding for mAbs (25)) makes achieving *in vitro* affinity maturation of these mAbs is difficult using standard approaches.

To date, relatively few successful attempts at *in vitro* affinity maturation of anti-glycan mAbs have been reported (26–35). Most of these efforts have targeted glycans that are easier to purify and lack the variable, highly repetitive architecture of polysaccharides like O-Ag or capsular polysaccharide. To our knowledge, the only bacterial O-Ag or capsular polysaccharide for which successful *in vitro* affinity maturation has been reported is the O-Ag from *Salmonella* serogroup B. However, the impact that improving the affinity of these mAbs had on antibacterial effector functions was not explored (32,33,36). As a result, the relationship between antibody binding affinity and the potency of specific effector functions is less well characterized for mAbs against bacterial polysaccharides than for those against mammalian glycans.

Here, we utilize a creative whole-cell in-solution phage display panning strategy, coupled with next-generation sequencing, to overcome these challenges and improve the affinity of a prototypical anti-O-Ag mAb specific for *Shigella flexneri* serotype 3a. We demonstrate that one to two mutations are sufficient to not only improve potency across effector functions against the target serotype, *S. flexneri* 3a, but to also expand breadth to serotype 3b. Importantly, a lack of polyreactivity against other bacterial strains or common polyreactivity reagents such as single stranded DNA (ssDNA) indicates that these improvements in binding are specific. Interestingly, binding affinity and potency are generally correlated for most effector functions, but are not necessarily interdependent, particularly for complement-independent opsonophagocytosis. Altogether, these data provide a framework for affinity maturing mAbs against bacterial polysaccharides *in vitro* and demonstrate that (at least in this test case) few mutations are needed to significantly improve the breadth and potency of an anti-O-Ag antibody.

Results:

hFlex3a2 functions as a chimeric huIgG1, but not as an scFv

hFlex3a2 is a murine hybridoma IgG3 that binds to *S. flexneri* 3a O-Ag and can coordinate complement-mediated bacteriolysis of this serotype in an antibody bactericidal assay (37). We determined the sequence of this mAb (Table S1) and found that it has many of the properties commonly associated with anti-O-Ag mAbs. The putative variable gene segment of the heavy chain of hFlex3a2 differs from the germline segment IGHV1-4*02, its closest germline progenitor, by only four amino acids, while the putative variable gene segment of the light chain of hFlex3a2 is entirely identical to its closest germline segment IGKV5-39*01 (Figure 1A). The high degree of similarity to its closest predicted germline

progenitor suggests that immunizing mice with purified lipopolysaccharide (LPS) did not stimulate high levels of somatic mutation *in vivo.* The putative VH and VL genes were grafted onto the human IgG1 constant regions to create a chimeric huIgG1 and this antibody was confirmed by ELISA to bind to *S. flexneri* 3a outer membrane vesicles (OMVs) (Figure 1B), a proxy for the bacterial cell surface (38), as well as to coordinate complement-mediated bacteriolysis of *S. flexneri* 3a in a luminescent antibody bactericidal assay (L-ABA, Figure 1C). Additionally, hFlex3a2 was highly serotype-specific, binding to only the surface of *S. flexneri* 3a that expresses wildtype O-Ag, when screened against a panel of serotypes and an O-Ag knockout mutant (Figures S6A and 1D). Thus, the low level of somatic mutation, combined with its narrow breadth, make hFlex3a2 representative of a canonical mAb against a bacterial surface polysaccharide.

We sought to improve the affinity of hFlex3a2 against *S. flexneri* 3a O-Ag using phage display. Since hFlex3a2 would be displayed as an scFv, we wanted to confirm that the antibody retains functionality in this format. However, binding of *S. flexneri* 3a OMVs by hFlex3a2 in an scFv format could not be detected by ELISA (Figure 2A). This is not surprising, as scFvs often exhibit lower target affinity and are less stable than their IgG counterparts (39,40). In an attempt to restore function to hFlex3a2 as an scFv, we identified two residues in the framework region of the VH and one in the VL that were rare and thus may be potentially problematic (41). We mutated all three of these residues to the amino acid most frequently found at their respective positions when compared to a database of other murine antibodies. We called this new mAb hFlex3a2_v2 (Figure 1A). Two of these new mutations were away from the closest germline sequence, while the other reverted that position back to its predicted germline amino acid (Figure 1A). As an scFv, binding of hFlex3a2_v2 to *S. flexneri* 3a OMVs, but not to the unrelated antigen ovalbumin, was observed (Figure 2A). Antigen binding was further confirmed by surface staining, which demonstrated that hFlex3a2_v2 scFv, but not the original hFlex3a2 scFv binds to the surface of *S. flexneri* 3a (Figure 2B). Importantly, as a chimeric huIgG1, hFlex3a2_v2 exhibited antigen binding similar to the parent mAb, demonstrating that the rare residues we identified did not impact IgG antibody binding (Figure 2C). Since hFlex3a2_v2 retained binding as a huIgG1, and restored binding as an scFv, while retaining antigen specificity, affinity maturation by phage display was completed using the hFlex3a2_v2 background.

Whole-cell in-solution panning enriched for mutations in the VL

To test whether phage display can be used to identify single mutations that improve hFlex3a2_v2 affinity, we designed two double-barcoded site-saturated mutagenesis scanning libraries: one for VH and one for VL. Each library contained single amino acid substitutions besides a cysteine at every site of either the VH or VL, leading to total library sizes of 2,223 and 1,995 variants for the VH and VL libraries respectively. Flanking synonymous codons were used to barcode mutation sites, enabling bioinformatic identification of sampled positions for mutation enrichment analysis. Initial efforts to fix purified *S. flexneri* 3a lipopolysaccharide to a plate for selection via solid-phase panning were unsuccessful. Whole-cell in-solution panning was previously used to discover antibodies that bind to bacterial surface carbohydrates (42), and so we adopted a similar panning strategy for affinity maturing our existing O-Ag antibody (Figure 3A). The phage

185 display libraries were panned in solution for two rounds against either the target bacterium
186 *S. flexneri* 3a or *S. sonnei*, which is a closely related bacterium with an entirely different
187 O-Ag structure (43). Input and output page libraries were subsequently sequenced by
188 next-generation sequencing. We reasoned that variants enriched specifically after
189 panning against *S. flexneri 3a*, but not *S. sonnei*, were likely to exhibit improved binding
190 to the target relative to the parental mAb, and these variants could be evaluated further.
191 This approach also had some advantages over other panning strategies. Specifically, the
192 approach did not require large-scale purification of O-Ag, and the approach also allowed
193 for panning on O-Ag in its native conformation and abundance without any biochemical
194 modifications.
195
196 After two rounds of panning with the VH library, no enrichment of hFlex3a2_v2 variants
197 was detected (Figure S1A and S1B). In contrast, specific enrichment did occur for variants
198 in the VL library. Despite all the variants being of roughly equal abundance in the input
199 library, by the second round of panning, positively and negatively enriched variants were
200 identified when panned against *S. flexneri* 3a as well as *S. sonnei* (Figure 3B). After two
201 rounds of panning against *S. flexneri* 3a, a strong increase in the frequency of next-
202 generation sequencing reads for variant mutations mapping to residues that cluster
203 around the VL CDRs was observed (Figure 3C). This enrichment was driven by the
204 accumulation of reads mapping to either a single variant or a subset of variants at these
205 sites (Figure S2). In some cases, such as at residue S30, a single variant was found to
206 dominate relative to other variants with mutations at that site, while at other residues,
207 such as N90, a few variants were found to be similarly abundant (Figure 3D). To
208 determine whether highly enriched variants identified during phage display screening
209 were of higher affinity than the parental antibody, we picked four variants — S30, L33,
210 A51, and N90 — for further investigation. We chose these variants because all four had
211 large increases in read frequencies after panning, suggesting that these residues may be
212 important. Additionally, each variant was specifically enriched following panning against
213 *S. flexneri* 3a relative to *S. sonnei* (Figures 3E and S3 and Table 1). Lastly, these variants
214 are located in or adjacent to CDRL1 (S30 and L33), CDRL2 (A51) or CDRL3 (N90). Since
215 no variants in the VH were enriched for, we will refer to the hFlex3a2_v2 variants solely
216 by their VL mutation(s) from here on.
217
218 **Variants enriched in phage display improve mAb binding to *S. flexneri* 3a O-Ag as**
219 **chimeric huIgG1s**
220 We hypothesized that the selected variants of hFlex3a2_v2 that were highly enriched
221 against *S. flexneri* 3a but not *S. sonnei* (S30G, L33N, A51R, and N90H) were likely to
222 have genuinely higher affinity against *S. flexneri* 3a O-Ag relative to the parent mAb. For
223 a comparison, we chose one additional variant — H34A — that was highly enriched
224 against both *S. flexneri* 3a and *S. sonnei* (Figures 3D, 3E, S3, and Table 1). All the
225 selected variants were produced as chimeric huIgG1s for further characterization (Table
226 1).
227
228 Surface staining showed that all the variants retained their ability to bind to the surface of
229 *S. flexneri* 3a (Figure 4A). Titration ELISA also confirmed binding to *S. flexneri* 3a OMVs
230 (Figure 4B) and showed that all four of the variants that were specifically enriched against

231 *S. flexneri* 3a (S30G, L33N, A51R, and N90H) had higher apparent affinities than their
232 parental mAb hFlex3a2_v2, while the variant that was enriched against both *S. flexneri*
233 3a and *S. sonnei* (H34A) had a lower apparent affinity (Figure S4A). The ELISA binding
234 curves were used to calculate EC_{50s} (Table 1 and Figure 4C). The parent mAb
235 hFlex3a2_v2 had an EC_{50} of 57.81 nM. L33N, the variant with the highest apparent
236 affinity, had an EC_{50} of 4.99 nM, while variant H34A had the lowest apparent affinity (EC_{50}
237 205.09 nM). This is consistent with the hypothesis underlying our panning strategy, that
238 specific enrichment against *S. flexneri* 3a provides a means of identifying variants that
239 improve target affinity.
240
241 We next wanted to determine whether combining the most beneficial single amino acid
242 mutations — S30G, L33N, and A51R — would synergize with one another to further
243 improve the affinity of hFlex3a2_v2. We constructed all the possible double and triple
244 combinatorial mutants. Since all the combinatorial variants retained their ability to bind *S.*
245 *flexneri* 3a (Figure 4A), we performed ELISA to determine their apparent affinities. All of
246 the combinatorial variants except L33N + A51R had synergistic improvements in apparent
247 affinity, meaning that the combinatorial variant had a lower EC_{50} than that of any single
248 mutation contained in the combination (Table 1, and Figures 4B, 4C, and S4A). Variant
249 S30G + L33N was the most potent binder, with an EC_{50} = 2.56 nM. We also tested a
250 variant combining all 5 of the single mutations and found that its apparent affinity (EC_{50} =
251 201.35 nM) was similar to that of H34A alone, suggesting that the presence of mutation
252 H34A may be dominantly detrimental over the other beneficial mutations. Due to the
253 oligomeric structure of O-Ag, it is difficult to accurately measure its molar concentration
254 in solution, complicating efforts to precisely measure the binding kinetics between the
255 mAbs and purified O-Ag *in vitro*. However, biolayer interferometry (BLI) confirmed that
256 the parent mAb, and the most potent and least potent variants in ELISA, S30G + L33N
257 and H34A respectively, can all bind purified *S. flexneri* 3a O-Ag (Figure 4D). Consistent
258 with the selected mutations affecting binding behavior, at both concentrations of O-Ag
259 tested, S30G + L33N reached a higher plateau in BLI than the parental mAb, while H34A
260 reached a lower plateau. Lastly, a panel of polyspecificity reagents were used in ELISA
261 to demonstrate that the mAb variants had limited polyreactivity against the antigens
262 tested, confirming that the better binding variants retained their antigen specificity (Figure
263 S4B).
264
265 **Improving binding of hFlex3a2_v2 enhances effector and anti-virulence functions**
266 To probe the relationship between improved O-Ag affinity and potency across
267 antibacterial functions, we tested our panel of hFlex3a2 variants in a series of effector
268 function and virulence assays. A Luminescent Antibody Bactericidal Assay (L-ABA),
269 which measures the ability of antibodies to coordinate complement-mediated
270 bacteriolysis, showed that the parent antibody was already potent at this effector function
271 (IC_{50} = 1.86 nM, Table 1, Figures 5A and S5A). Nonetheless, the best binding single
272 amino acid variant, L33N, modestly but reproducibly improved upon the parent mAb
273 (IC_{50}= 1.32 nM, p=0.04), while the best binding combinatorial variant, S30G + L33N, had
274 a more substantial ~2.7-fold improvement in potency (IC_{50} = 0.68 nM, $p<0.0001$). The
275 worst binding variant H34A had the weakest potency in L-ABA (IC_{50} = 4.86 nM, $p<0.0001$),
276 showing that binding strength and *in vitro* complement-mediated bacteriolysis are

277 correlated (R^2=0.91, Figure S5B). Similarly, when hFlex3a2_v2 was tested in a
278 complement-independent opsonophagocytosis assay (OPA) at a 30 nM concentration,
279 17.7% of monocytes were cell trace violet positive (CTV+), indicating that they had
280 phagocytosed *S. flexneri* 3a that was opsonized with this mAb (Figure 5B). The gating
281 strategy for OPA is shown in Figure S4C. Although hFlex3a2_v2 already had the ability
282 to facilitate OPA activity, L33N, the best binding single amino acid variant, was almost 2-
283 fold more potent at the same concentration (33.7% CTV+, p = 0.02). The best binding
284 combinatorial variant S30G + L33N was the most potent at facilitating OPA (38.6% CTV+,
285 p <0.005). Despite having little improvement in binding and L-ABA compared to the
286 parental mAb, variant N90H was the third most potent in OPA (32.2% CTV+, p = 0.04).
287 Similarly, despite exhibiting lower apparent affinity, H34A and the combination of all 5
288 mutations had similar potency in OPA to the parent antibody at 30 nM (Figure 5B). This
289 demonstrates that, while largely correlated, other factors beyond binding strength also
290 impact O-Ag mAb function in the OPA.
291
292 In addition to promoting effector functions that modulate the immune system, mAbs can
293 also directly neutralize bacterial virulence. As an intracellular pathogen, invasion of
294 colonic epithelial cells is an indispensable step in the pathogenesis of *S. flexneri*. An *in*
295 *vitro* invasion assay showed that, relative to PBS or a non-binding control mAb,
296 hFlex3a2_v2 does not significantly block *S. flexneri* 3a invasion of a monolayer of HeLa
297 cells (Figure 5C). However, the highest affinity single amino acid variants and
298 combinatorial variants all blocked *S. flexneri* 3a invasion by at least 60% (Figure 5C). This
299 demonstrates that for anti-O-Ag antibodies, increasing affinity can help to directly
300 neutralize bacterial virulence.
301
302 **Improving affinity of hFlex3a2_v2 against *S. flexneri* 3a increases its functional**
303 **potency against *S. flexneri* 3b**
304 Lastly, we wanted to determine whether higher affinity variants of hFlex3a2_v2 would also
305 have increased breadth compared to their parent mAb. Although the precise epitope of
306 hFlex3a2_v2 is not known, we reasoned that many of the components of *S. flexneri* 3a
307 O-Ag are also found in the O-Ag of other *S. flexneri* serotypes, and some of the variants
308 may have increased affinity against some O-Ag component common to other *S. flexneri*
309 serotypes. We performed a surface staining experiment with a panel of *S. flexneri*
310 serotypes that all share the same core O-Ag sugars, but with different modifications, as
311 well as *S. sonnei*, which has an entirely unrelated O-Ag composition (Figure 6A). As
312 previously shown, all hFlex3a2_v2 variants bound to *S. flexneri* 3a and binding to a
313 mutant *S. flexneri* 3a O-Ag- strain (Figure S6A) was 10-fold lower than to *S. flexneri* 3a
314 that expresses wildtype O-Ag, confirming that O-Ag is necessary for binding. For all the
315 hFlex3a2 variants tested, no reactivity to *S. flexneri* serotypes 1b, 2a, 2b, Y, or *S. sonnei*
316 was observed (Figure 6B). In contrast, surface staining against *S. flexneri* 3b showed that
317 hFlex3a2_v2 weakly cross-reacts with this serotype. The single amino acid variant L33N
318 and the combinatorial variant S30G + L33N had surface staining median fluorescence
319 intensities that were 4-fold and 5.7-fold higher, respectively.
320
321 Since surface staining experiments showed that the higher affinity variants of
322 hFlex3a2_v2 bind to *S. flexneri* 3b, we wanted to further characterize their effect on

323 binding and effector function. ELISA measuring binding to *S. flexneri* 3b OMVs, in
324 agreement with the surface staining experiment, showed that hFlex3a2 weakly binds to
325 *S. flexneri* 3b O-Ag (Figure 6C and Figure S6B). The variants showed the same pattern
326 in relative apparent affinities as against *S. flexneri* 3a. Specifically, single amino acid
327 variants S30G, L33N, and A51R all increased apparent affinity. N90H bound similarly to
328 the parent antibody and H34A had a lower apparent affinity than the parent antibody. All
329 combinations of the beneficial single mutations were found to be synergistic except for
330 L33N + A51R. The combination of all 5 mutations bound poorly, similarly to H34A alone.
331 The best binding single mutation was L33N, and the best binding combinatorial mutation
332 was S30G + L33N, which had EC_{50} values of 322.5 nM and 165.3 nM respectively. We
333 next wanted to determine whether these improvements in affinity for *S. flexneri* 3b O-Ag
334 are sufficient to drive effector functions against this serotype. We compared the parent
335 mAb to the best binding single variant, L33N, and the best binding combinatorial variant,
336 S30G + L33N, in an L-ABA assay. In this assay, hFlex3a2_v2 displayed weak
337 complement-mediated bactericidal activity against serotype 3b, only reaching 37% killing
338 at 90 nM, the highest concentration of antibody tested (Figure 6D). Both the single L33N
339 mutation and combination of S30G + L33N mutations were more potent in this assay, with
340 IC_{50} values of 30.4 nM and 18.0 nM, respectively. Similarly, in an OPA assay,
341 hFlex3a2_v2 was able to facilitate opsonophagocytosis at a concentration of 30 nM,
342 leading to 7.4% CTV+ monocytes (Figure 6E). At the same concentration of mAb, the
343 most potent single amino acid variants were ~3-fold more potent at OPA, while the most
344 potent combinatorial variants were ~4.5-fold more potent (Figure 6E). However, despite
345 improving affinity and potency in effector function assays, the higher affinity variants of
346 hFlex3a2_v2 did not block *S. flexneri* 3b invasion (Figure 6F). Together, this data shows
347 that panning against *S. flexneri* 3a was able to increase the functional breadth of this
348 antibody to also exhibit effector functions against *S. flexneri* 3b, likely by improving the
349 affinity to a shared epitope on these two serotypes that was weakly recognized by the
350 parent mAb.
351
352 **Discussion**
353 Here, we report the development of a panning strategy that enabled the rapid affinity
354 maturation of a mAb against the O-Ag of *S. flexneri* 3a. We demonstrate that variants with
355 improved affinity exhibit more potent effector functions against both *S. flexneri* 3a and the
356 related but distinct serotype *S. flexneri* 3b. By pairing whole-cell in-solution panning with
357 NGS and using both the target bacterial strain and a related strain with a completely
358 unrelated O-Ag, we were able to efficiently identify specific mutations that could increase
359 affinity against the target strain. It is notable that out of the four tested variants that met
360 the criteria for specific enrichment (S30G, L33N, A51R, and N90H), three of them (S30G,
361 L33N, A51R) improved affinity by ELISA, and all four exhibited improved potency in at
362 least one effector function assay. One of these mutations, L33N, was sufficient to
363 increase apparent affinity in ELISA by approximately 10-fold over the parent mAb, which
364 is comparable to what has been reported for germline mAbs against *Chlamydia* core
365 lipopolysaccharide (28). In contrast, H34A, which was enriched against both bacterial
366 species (possibly indicating that this mutation improves a non-specific parameter such as
367 display efficiency on phage), had lower affinity than the parent, supporting the rationale
368 of this approach.

369
370 Unexpectedly, while variants in the hFlex3a2 VL library were successfully enriched
371 following panning, no variants were enriched from the VH library (Figure S1). It is possible
372 that the VH is already optimized, and we were simply unable to find point mutations that
373 conferred additional advantage. This is supported by the observation that, while the VL
374 protein sequence of hFlex3a2 is identical to germline, the VH sequence already contains
375 somatic mutations that result in four amino acid substitutions (Figure 1A). However, the
376 fact that no enrichment was observed against either *S. flexneri* 3a or *S. sonnei* (which
377 would not be expected, as at least some variants should be nonspecifically enriched for
378 reasons of improved display efficiency or scFv stability), leaves open the possibility that
379 this was a technical issue with the panning process rather than a biological one. Further
380 experiments would be needed to definitively determine whether any additional VH
381 mutations can further improve binding and function of hFlex3a2. The identification and
382 characterization of VH mutations that further synergize with the already identified VL
383 mutations will be of interest in future studies.
384
385 As expected, higher affinity hFlex3a2 variants were generally more potent across all
386 assays (Figure 5), with some notable exceptions. In L-ABA, affinity was tightly correlated
387 with potency (Figure S5B), suggesting that potency in this assay has a linear relationship
388 with affinity. Similarly, higher affinity variants were able to block invasion by *S. flexneri* 3a,
389 while the parent mAb was not (Figure 5C). However, even these enhanced variants were
390 unable to block invasion by serotype 3b (Figure 6F). While it is possible that the
391 mechanism of action by which hFlex3a2 and its variants are inhibiting *S. flexneri* 3a
392 invasion is not applicable to *S. flexneri* 3b, we suspect that this observation is more likely
393 due to invasion inhibition requiring a greater affinity than L-ABA or OPA activity. Even
394 though some hFlex3a2_v2 variants are more potent against *S. flexneri* 3b than the
395 parental mAb, the best variants have weaker affinity and potency against serotype 3b
396 than 3a. Given the inherent biological variability of the invasion assay compared to L-ABA
397 or OPA, and that the parent mAb does not measurably inhibit invasion against even 3a,
398 we think that the best variants simply lack sufficient affinity to reach the threshold where
399 a decrease in invasion by 3b is consistently measurable in this assay. It is possible that
400 panning against 3b with the hFlex3a2_v2 library would identify variants that further
401 improve activity against this serotype.
402
403 The relationship between OPA and affinity was more complex than those between affinity
404 and the L-ABA or invasion assay. While the highest affinity variants tested here (L33N
405 and S30G + L33N) did exhibit higher degrees of opsonophagocytosis than the parent
406 mAb, N90H, which does not have detectably higher affinity and was not more potent in
407 L-ABA, also improved macrophage uptake of both *S. flexneri* 3a and 3b (Figure 5B and
408 6E). Similarly, H34A, which has lower affinity and L-ABA potency than the parent,
409 performed similarly to the parent mAb in the OPA (Figure 5B and 6E). A similar
410 phenomenon has been observed for some mAbs targeting the human immunodeficiency
411 virus (HIV) glycoprotein gp120 as they exhibit different capacities to drive antibody-
412 dependent cellular cytotoxicity against HIV-infected cells displaying gp120, despite being
413 from the same lineage, having the same affinity, and binding the same epitope (44). In
414 that study, it was proposed that these differences are a consequence of either subtle

415 variations in the structural recognition of the epitope or other changes in the binding
416 dynamics between the mAb and the antigen. We suspect similar factors, such as changes
417 in the kinetics of binding (but not necessarily equilibrium affinity) may allow N90H to
418 coordinate opsonophagocytosis more efficiently than the parent mAb despite having the
419 same apparent equilibrium affinity. Unfortunately, because purified *S. flexneri* 3a O-Ag is
420 present at a range of molecular weights, it is not currently possible to obtain accurate
421 kinetic measurements to test this hypothesis. However, future studies on the relationship
422 between affinity and effector function potency among mAbs against bacterial
423 polysaccharides may provide more mechanistic insights. Altogether, these data support
424 the hypothesis that higher affinity generally improves antibacterial function performance
425 for anti-O-Ag mAbs, with some notable exceptions and potential caveats.
426
427 Most importantly, this work informs the development of therapeutic mAbs targeting
428 bacterial polysaccharides. More test cases are required to establish the generalizability
429 of this approach. However, these data demonstrate that in principle, this whole-cell in-
430 solution panning approach can rapidly identify variants with improved affinity without the
431 need for antigen purification, and these improvements lead to direct functional
432 improvements. More interestingly, the observed enhancement of activity against *S.*
433 *flexneri* 3b suggests that if a mAb is targeting an epitope shared with other bacterial
434 serotypes, it may be possible to improve functional breadth alongside potency. This
435 supports the development of clinically relevant mAbs against bacterial polysaccharides,
436 because discovery campaigns can now prioritize mAbs that have relatively high breadth
437 by binding sugars common to many bacterial polysaccharides. Broad binders can then
438 be rapidly improved using this method. Future work will explore the potential of more
439 complex panning strategies that incorporate multiple serotypes, which can further
440 facilitate the identification of variants with improved breadth. Altogether, these results are
441 an important step towards expanding the mAb engineering toolkit for anti-polysaccharide
442 mAbs, which in turn may help develop novel therapeutics against AMR bacterial
443 pathogens.
444
445 **Materials and methods**
446 **Bacterial strains and growth conditions**
447 Bacterial strains and plasmids used in this study can be found in Table S2. *Shigella* strains
448 were maintained at -80 °C in tryptic soy broth (TSB) containing 20% (vol/vol) glycerol.
449 *Shigella* was grown aerobically at 37 °C on TSB agar with 0.01% Congo red dye.
450 For all assays, bacteria were grown in the desired medium overnight, then subcultured
451 1:100 into fresh growth medium and grown aerobically at 250 rpm, 37 °C.
452
453 **Cell culture conditions**
454 HeLa cells were grown in high glucose DMEM (Gibco) + 10% FBS + 2 mM glutamine and
455 1x Pen/Strep. THP-1 cells were grown in RPMI (Gibco) + 10% FBS + 10mM Hepes pH
456 7.4 + 1 mM Sodium Pyruvate + 55 µM beta-mercaptoethanol and 1x Pen/Strep. For
457 assays involving bacteria, HeLa and THP-1 cells were first washed into fresh media that
458 does not contain Pen/Strep. Expi293™ cells were grown in Expi 293™ Expression
459 Medium (Gibco).
460

461 **10x sequencing of hybridomas**
462 An unsequenced hybridoma expressing the mAb hFlex3a2, which was discovered and
463 described previously by WRAIR and collaborators (37), was provided to IAVI by WRAIR.
464 Single cells were isolated using a BD FACSMelody™ cell sorter, and heavy and light
465 chain variable domains were sequenced using the 10X single cell genomics platform (10X
466 Genomics, Inc.). Sequence analysis to predict CDRs, align to germline, and identify rare
467 residues was done using IMGT/V-Quest, IgBLAST, and abYsis (45–47). The VH and VL
468 sequences were cloned into a modified pcDNA3.2 expression vector and purified as full
469 IgG as described below. The mAb was confirmed to have properties consistent with the
470 parental hybridoma mAb (Figure 1).
471
472 **Construction of plasmids**
473 Primers and plasmids used in this study can be found in Table S3. For periplasmic
474 expression of scFvs, hFlex3a2 and hFlex3a2_v2 were designed as scFvs in the following
475 orientation — PelB signal sequence, hFlex3a2 VH, (GGGGS)3X linker, hFlex3a2 VL —
476 ordered as gBlocks (Integrated DNA Technologies), then cloned between the NcoI and
477 BamHI restriction sites of the bacterial expression vector pET28b (+) using NEBuilder®
478 HiFi DNA Assembly following the manufacturer's instructions (New England Biolabs). For
479 expression as huIgG1, the variable regions of hFlex3a2 and hFlex3a2_v2 were cloned
480 into a pcDNA3.2-based human antibody expression vectors containing the relevant
481 huIgG1 or Ig kappa constant domains. For single amino acid mAb variants, primers were
482 designed to insert the mutations into the appropriate VL sequence by HiFi DNA Assembly
483 (New England BioLabs). Combinatorial variants of hFlex3a2 and hFlex3a2_v2 VL chains
484 were ordered as gBlocks and inserted into the appropriate human antibody expression
485 vector using NEBuilder® HiFi assembly.
486
487 **Construction of *Shigella* mutants**
488 *Shigella flexneri* 3a and 3b *tolR* mutants that hyperproduce OMVs (48), and *S. flexneri* 3a
489 *waaL* mutant (O-Ag knockout) (49) were produced by the gene-gorging method as
490 previously described (50). Briefly, a mutation cassette consisting of 500 bp of *Shigella*
491 genomic DNA upstream of the target mutation site, the kanamycin resistance gene from
492 plasmid pKD4, and 500 bp of DNA downstream of the target mutation site, flanked on
493 both sides of the mutation cassette by the restriction site I-SceI was constructed using
494 splice by overlap extension PCR (51). The mutation cassette was A-tailed and ligated into
495 the plasmid pGEM®-T Easy (Promega) to create a donor plasmid. The donor plasmid
496 was electroporated into the desired *S. flexneri* strain that had previously been
497 electroporated with plasmid pACBSR. Strains containing both the donor plasmid and
498 pACBSR were grown for 6 hours at 30 °C in LB + chloramphenicol + 0.4% arabinose to
499 induce genomic recombination and then plated on TSBA + Kanamycin for single colonies.
500 Colonies were passaged multiple times at 37 °C to promote the loss of pACBSR. After
501 multiple passages, colonies were confirmed to be kanamycin resistant but
502 chloramphenicol sensitive, indicating loss of donor plasmid, and the successful insertion
503 of the genomic mutation was verified by Sanger sequencing.
504
505 **Phage library construction and panning**

506 Double-barcoded site-saturated mutagenesis scanning libraries of the VL and VH of
507 hFlex3a2_v2 were designed and ordered from Twist Biosciences. The libraries were
508 amplified with primers to introduce SfiI sites and then ligated into the SfiI site of phagemid
509 pCOMB3XSS (52). To produce phage, the phagemid libraries were electroporated into
510 XL1-Blue (Agilent), recovered in 5 mL of SOC, and then grown (37 °C, 250 RPM) to OD_{600}
511 ~0.5 in 10 mL of Super Broth + Tet + Carb before being super infected with M13ko7 helper
512 phage (New England Biosciences) at an MOI of 20, expanded, and grown overnight (30
513 °C, 250 rpm) in 200 mL of super broth + Tet + Carb + Kan.
514
515 Phage was precipitated from the supernatant with 0.5 M NaCl and 4% PEG-8,000 as
516 previously described (53) and then panned against whole bacteria in-solution, based on
517 a previously published method (42). Briefly, 1 x 10^9 cfu of *S. flexneri* 3a or *S. sonnei* were
518 blocked in 3% nonfat milk in PBS and then each bacterial species was incubated with 5
519 x 10^{10} pfu of blocked phage particles for 15 min to 2 h. Non-binding phage was washed
520 5x with PBS + 5% Tween-20 after round 1 of panning and washed 10x after round 2.
521 Binding phage was eluted by mixing with 0.1 M HCl pH 2.2 (pH adjusted with glycine) for
522 ten minutes at room temperature, then neutralized with 2 M Tris base and used to reinfect
523 XL1-Blue cells to generate phage for the second round of panning. XL1-Blue containing
524 the input library, post-panning round 1 phagemids, and post-panning round 2 phagemids
525 were maxiprepped, the variable chain sequences were PCR-amplified and deep-
526 sequenced by MiSeq (Illumina) using Amplicon-EZ platform (Genewiz). The relative
527 enrichment of phage library variants against *S. flexneri* 3A and *S. sonnei* after rounds 1
528 and 2 of panning was quantified using an in-house Python script.
529
530 **Antibody and antigen purification**
531 For purification of IgGs, Expi293 cells were co-transfected with the desired heavy chain
532 and light chain pair at a ratio of 1:2.5 with FectoPRO® (Polyplus) in Expi293™ Expression
533 Medium (Gibco). The cells were supplemented with 3 mM valproic acid (Sigma-Aldrich)
534 and 0.4% D-(+)- glucose (Sigma-Aldrich) 24 h after transfection. The supernatant was
535 harvested on day 5 post-transfection, IgGs were purified using Praesto AP+ agarose resin
536 (Purolite), and then buffer exchanged and concentrated using 30 kDa cutoff spin filter
537 (Amicon).
538
539 scFv purification was based on a previously described method (54). Briefly, BL21
540 containing the desired scFv cloned into pET28b (+) was grown to OD_{600} 0.6-0.8 in terrific
541 broth (37 °C, 250 rpm) and then induced with 1 mM IPTG overnight (18 °C, 250 RPM).
542 Bacteria were collected, resuspended in 40 mL of TES buffer (0.5 M Sucrose, 0.5 mM
543 EDTA, and 0.2 M Tris-HCl pH 8.0), incubated at 4 °C for 30 min, and then osmotically
544 shocked with 80 mL of ice-cold ddH_2O for 1 h at 4 °C. Lysed bacteria were pelleted, the
545 supernatant was collected, adjusted to 150 mM NaCl, 2 mM $MgCl_2$, 20 mM imidizaole,
546 and incubated with 1 mL of Ni-NTA resin (Anatrace) at 4 °C for at least 1.5 h. scFv bound
547 resin was packed onto gravity columns, washed extensively with wash buffer (150 mM
548 NaCl, 2 mM $MgCl_2$, 30 mM imidazole), and then eluted with elution buffer (150 mM NaCl,
549 2 mM $MgCl_2$, 300 mM imidazole) before buffer exchanging and concentrating with PBS
550 using a 10 kDa cutoff centrifugal filter (Amicon).
551

552 To purify OMVs, supernatant was collected from *S. flexneri* 3a or 3b tolR::kan mutants
553 grown overnight in SSDM (48) supplemented with 40 mg/L l-methionine and 20 mg/L
554 tryptophan. The supernatant was filter-sterilized through a 0.2 µM filter (Sartorius) and
555 then concentrated to ~ 50 mL by tangential flow filtration using a Vivaflow® 100 kDa cutoff
556 filter (Sartorius®). The concentrated supernatant was ultracentrifuged at 200,000 x g for
557 1.5 h to pellet OMVs, which were then resuspended in 1 mL of PBS and stored at -20 °C
558 for future use. Total protein content of OMVs was quantified by Micro-BCA™ assay
559 (Thermo Fisher) following the manufacturer's instructions. OMV amount was normalized
560 by total protein content for ELISA assays.
561
562 O-Ag was purified from whole bacteria by acetic acid hydrolysis (55). Acetic acid was
563 added at a final concentration of 2% to a culture of stationary phase *S. flexneri* 3a and
564 incubated at 100 °C for 5 h. After hydrolysis, the culture was neutralized to pH ~ 6 with
565 ammonium hydroxide (Sigma-Aldrich). Bacterial debris was pelleted, the supernatant was
566 buffer exchanged by tangential flow filtration using a VivaFlow 30 kDa cutoff filter
567 (Sartorius) first into 1 M NaCl, and then into ddH_2O.The buffer exchanged supernatant
568 was concentrated to ~50 mL. Citrate buffer (20 mM, pH 3) was added to the supernatant,
569 and it was incubated at room temperature for 30 min, centrifuged at 12,000 x g for 30 min
570 and then passed through a Sartobind® IEX S75 cationic exchange filter (Sartorius). After
571 cation exchange, the supernatant was precipitated once more with 18 mM Na_2HPO_4, 24%
572 ethanol, and 200 mM $CaCl_2$ at room temperature for 30 min, then buffer exchanged as
573 described above before being concentrated to approximately 1 mL in ddH_2O using a 30
574 kDa cutoff spin filter (Amicon). The purified O-Ag was quantified using a Total
575 Carbohydrate Assay Kit (Sigma-Aldrich) following the manufacturer's instructions.
576 Contaminating DNA and protein levels were assessed by nanodrop analysis and Micro-
577 BCA™ assay, respectively, and confirmed to be at least 10-fold lower than carbohydrate
578 concentration.
579
580 **ELISA assays**
581 All ELISA assays were performed in 384-well high binding ELISA plates (Corning). Wells
582 were coated overnight at 4 °C with antigen in PBS at a concentration of 2.5 µg/mL for
583 OMVs or 5 µg/mL for ovalbumin, CHO-SMP, insulin, and ssDNA. Antigen-coated wells
584 were blocked in PBS containing 3% BSA and 0.05% Tween-20 at 37 °C for 1 h. Antibodies
585 to be tested were diluted in 1% BSA + 0.017% Tween-20 at the desired antibody
586 concentration and incubated with the blocked antigen at 37 °C for 1 h. After incubation
587 with the test antibody, wells were washed 3x with PBS + 0.05% Tween-20 and incubated
588 with the appropriate secondary antibody at room temperature for 1 h. Secondary
589 antibodies used were either AP-conjugated anti-Flag M2 (Sigma-Aldrich) for scFvs or AP-
590 conjugated anti-Human Fc (Jackson ImmunoResearch) for huIgG1s, both at a 1:1000
591 dilution in PBS + 1% BSA + 0.017% Tween-20. After washing three times more, AP
592 substrate tablets (Sigma-Adrich) were dissolved and diluted to 1 mg/mL in AP buffer (50
593 mM $MgCl_2$, 100 mM NaCl, 1%Tween 20). ELISAs were developed with AP substrate (20
594 min for IgGs or 40 min for scFvs) at room temperature. Absorbance at 405 nm was read
595 on a BioTek Synergy microplate reader.
596
597 **Luminescent Antibody Bactericidal Assays (L-ABA)**

598 L-ABA was adapted from previously published protocols (37,56). Briefly, the desired *S.*
599 *flexneri* serotype was grown to mid-log phase in TSB (BD Biosciences) and resuspended
600 at a concentration of 3 x 10^5 CFU/mL in 100 µL of assay buffer (HBSS + 0.1% Gelatin,
601 pH 7.4) with 7.5% Baby Rabbit Complement (Pel-Freez Biologicals), and the test antibody
602 at the desired concentration. The L-ABA reaction was incubated for 3 h at 37 °C, washed
603 once with 100 µL of fresh assay buffer, mixed 1:1 with BacTiter-Glo™ (Promega), and
604 incubated for 5 min at room temperature. Luminescence was read on a BioTek Synergy
605 plate reader. Adalimumab (57) expressed as a chimeric macaque IgG1 was used as a
606 control mAb. To normalize for differences in bacterial growth, the data was fit with a
607 sigmoidal four parameter logistic curve on GraphPad Prism, and each curve was
608 normalized to the Top best-fit value of their curve to determine their fraction maximal
609 luminescence.
610
611 **Opsonophagocytosis Assays (OPA)**
612 For OPA, the desired *S. flexneri* strain was grown to OD_{600} of approximately 0.5 in TSB,
613 washed with PBS, and stained with a 1:50 dilution of CellTrace™ Violet (CTV, Thermo
614 Fisher) for 15 min at 37 °C. Excess dye was quenched with FACS buffer (PBS + 1%
615 FBS), the bacteria were washed in PBS and resuspended in assay buffer (HBSS + 0.1%
616 gelatin, pH 7.4). 2.5 x 10^6 CFU of bacteria were mixed with the desired concentration of
617 mAb in assay buffer and incubated at 37 °C for 30 min. Opsonized bacteria were then
618 mixed with 5 x 10^4 THP-1 cells and incubated for 30 min at 37 °C in 5% CO_2. After 30
619 min, the OPA reactions were stained on ice in the dark for 30 min with Live/Dead Near-
620 IR dye (Thermo Fisher) diluted 1:2000 in PBS and FITC-conjugated anti-CD45 antibody
621 (BD Biosciences) diluted 1:4000. The cells were then fixed with 4% PFA for 30 min, on
622 ice. To determine relative OPA activity, the percentage of THP-1 cells incubated with *S.*
623 *flexneri* opsonized with the mAbs of interest that were Near IR-, CD45+, and CTV+ was
624 quantified by flow cytometry using a FACSCelesta (BD Biosciences).
625
626 **Invasion Assays**
627 Invasion was measured by a gentamicin protection assay (58). *S. flexneri* was grown to
628 an OD_{600} of approximately 0.7 in TSB (37 °C, 250 RPM), washed in PBS, resuspended
629 at a concentration of 1 x 10^9 CFU/mL, and incubated with 1 µM of the desired mAb or
630 PBS (control) for 30 min at 37 °C. 10 µL of bacteria (~1 x 10^7 CFU, MOI = 20) was added
631 to a monolayer of approximately 5 x 10^5 HeLa cells in a tissue culture-treated 24-well
632 plate (Corning) and centrifuged at 900 x g for 10 min. The plate was incubated for 30 min
633 at 37 °C and 5% CO_2, washed two times with PBS, the media was replaced with DMEM
634 containing 25 µg/mL gentamicin, and the plate was incubated for an additional 1 h. The
635 wells were washed twice more with PBS and then lysed with 0.1% Triton X-100. Serial
636 dilutions of the mAb-treated and control bacteria were plated, and percent invasion was
637 calculated. Adalimumab (57) expressed as a chimeric macaque IgG1 was used as a
638 control mAb.
639
640 **Bacterial surface staining**
641 To measure bacterial surface staining, *S. flexneri* was grown to an OD_{600} of approximately
642 0.5, washed and resuspended in PBS to a concentration of 2 x 10^9 CFU/mL. The desired
643 mAb was added to 25 µL of bacteria at a final concentration of 50 nM and incubated at

644 37 °C for 30 min. The bacteria were washed with PBS and then incubated with a 1:100
645 dilution of the appropriate secondary antibody for 30 min at room temperature. For scFvs,
646 the secondary antibody was Alexa Fluor 647-conjugated anti-Flag antibody (Abcam), and
647 for huIgGs this was BV421-conjugated anti-Human IgG (BD Biosciences). Bacteria were
648 then fixed with 4% PFA for 30 min on ice. Median fluorescence intensity was determined
649 by flow cytometry on a FACSSymphony A5 (BD Biosciences).
650
651 **Biolayer interferometry**
652 Binding of hFLex3a2_v2 variants to *S. flexneri* 3a O-Ag was characterized by BLI using
653 an Octet® R8 (Sartorius) with Octet AHC Biosensors (Sartorius). All antibodies and
654 antigens were in PBS + 0.02% Tween-20 + 0.01% BSA. The BLI protocol was as follows:
655 300 seconds baseline, 120 seconds loading with 1 μM mAb, 180 seconds baseline, 360
656 seconds association with 100 μg/mL of *S. flexneri* 3a O-Ag or 540 seconds with 20 μg/mL
657 of *S. flexnei* 3a O-Ag, and 600 seconds dissociation. BLI results were analyzed on Octet
658 Analysis Studio (Sartorius) and plotted with GraphPad Prism. hFlex2a1 (37) expressed
659 as a chimeric huIgG1 was used as a control mAb.
660
661 **O-Ag visualization**
662 To visualize O-Ag, crude protein-free LPS extract was purified from *S. flexneri* 3a and *S.*
663 *flexneri* 3a waaL::kan (O-Ag-) following the method of Darveau and Hancock (59).
664 Bacterial LPS extract was separated by SDS-PAGE and stained with Pro-Q™ Emerald
665 300 Lipopolysaccharide Gel Stain Kit (Thermo Fisher) following the manufacturer's
666 instructions. Stained gels were visualized on a ChemiDoc MP Imaging System (Bio-Rad).
667
668 **Fig 1: Analysis of binding and function of putative hFlex3a2 as a huIgG1 chimera.**
669 (A) Alignment of putative hFlex3a2 VH and VL protein sequences to their closest germline
670 progenitors shows high levels of similarity. Residues that were modified to create mAb
671 hFlex3a2_v2 are denoted by (*). Alignment and CDR predictions were determined with
672 IMGT/V-Quest and rare residues were identified with abYsis (45,46). (B) Titration ELISA
673 measures the binding of increasing concentrations of hFlex3a2 huIgG1 to 2.5 μg/mL of
674 *S. flexneri* 3a OMVs. This experiment is the average of three independent replicates each
675 performed in duplicate. (C) L-ABA measuring the ability of increasing concentrations of
676 hFlex3a2 huIgG1 and a non-binding control mAb, to coordinate complement-mediated
677 bacterial killing of *S. flexneri* 3a. L-ABA is the average of three biological replicates
678 performed in duplicate. (D) Surface staining with 50 nM of mAb shows that hFlex3a2, and
679 not a non-binding control mAb, binds specifically to *S. flexneri* 3a wildtype O-Ag. This
680 experiment is the average of three experimental replicates. Error bars represent standard
681 deviation.
682
683 **Fig 2: Analysis of binding of hFlex3a2 and hFlex3a2_v2 as an scFv.** (A) Titration
684 ELISA shows that at concentrations above 100 nM of scFv, hFlex3a2_v2, but not
685 hFlex3a2, binds to *S. flexneri* 3a OMVs (2.5 μg/mL). Neither scFv bound to the unrelated
686 antigen ovalbumin (5 μg/mL). This experiment was repeated three times, and a
687 representative experiment is shown. (B) Titration ELISA of hFlex3a2_v2 reformatted as
688 a chimeric huIgG1 and the original hFlex3a2 huIgG1 shows similar binding to *S. flexneri*
689 3a OMVs (2.5 μg/mL). This experiment is the result of two independent replicates. (C)

690 Surface staining confirms that in the scFv format, hFlex3a2_v2, but not hFlex3a2, binds
691 *S. flexneri* 3a. scFvs were tested at a concentration of 1μM. This experiment represents
692 two replicates. Error bars represent standard deviation.
693
694 **Fig 3: Whole-cell in-solution panning enriches for VL variants.** (A) Whole-cell in-
695 solution panning strategy. To identify better binding variants of hFlex3a2_v2 scFv, we
696 panned a phage-displayed site-saturated mutagenesis scanning library of VL or VH
697 against either *S. flexneri* 3a or *S. sonnei* in-solution for two rounds and sequenced output
698 phage by next-generation sequencing to identify variants that were specifically enriched
699 against *S. flexneri* 3a. (B) log10 enrichment of variants in the VL library after two rounds
700 of panning against *S. flexneri* 3a and *S. sonnei*. Dotted line is 20 standard deviations
701 above the mean mutation enrichment in the input library and indicates a stringent
702 threshold set to distinguish bacteria-mediated enrichment from background variability. (C)
703 Fold-change in the frequency of next-generation sequencing reads for variant mutations
704 at each site on hFlex3a2_v2 VL after panning, relative to their frequency in the initial
705 library, shows that certain residues that cluster in and around the CDRs have a large
706 increase in read frequency. (D) The percent distribution of all variants for each site of the
707 CDRs after two rounds of panning against *S. flexneri* 3a shows that at some sites (I29,
708 S30, H34) a single variant, or at other sites (L33, A51, N90, S93) a handful of variants
709 were enriched for. (E) Specificity of mutational enrichment was determined. Each dot
710 represents the enrichment of a variant against *S. flexneri* 3a relative to *S. sonnei* at the
711 indicated residue after two rounds of panning. Positive numbers indicate variants that
712 were enriched against *S. flexneri* 3a relative to *S. sonnei*, zero indicates similar
713 enrichment against both bacterial species, and negative numbers indicate variants that
714 were enriched for against *S. sonnei* relative to *S. flexneri* 3a. Dotted line is 20 standard
715 deviations above the mean mutation enrichment in the input library.
716
717 **Fig 4: Binding analysis of hFlex3a2_v2 variants specifically enriched against *S.*
718 *flexneri* 3a and produced as huIgG1 chimeras** (A) Surface staining experiment
719 confirms that 50 nM of the parental mAb (red), single amino acid variants (green), and
720 combinatorial variants (blue) bind *S. flexneri* 3a ~100-fold higher than a non-binding
721 control mAb (black) as indicated by a median fluorescence intensity. Surface staining is
722 the average of three biological replicates. Error bars represent standard deviation. (B)
723 Binding curves from a titration ELISA against *S. flexneri* 3a OMVs (2.5 μg/mL) show
724 relative binding potencies of the parent mAb (red), single amino acid variants (green),
725 and combinatorial variants (blue). ELISA binding curves are the average of three
726 independent replicates each performed in duplicate (C) EC_{50} values calculated from the
727 ELISA in panel B show relative steady-state apparent affinities of hFlex3a2_v2 variants.
728 Black line indicates the median EC_{50}. (D) Binding of hFlex3a2_v2, H34A, S30G + L33N,
729 and a non-binding control as huIgG1s to purified *S. flexneri* 3a O-Ag was assessed by
730 BLI. This experiment is the average of two experiments performed with independently
731 purified batches of mAbs.
732
733 **Fig 5: Functional analysis of hFlex3a2_v2 variants against *S. flexneri* 3a.** (A) L-ABA
734 assay comparing the ability of hFlex3a2_v2 variants and a non-binding control to
735 coordinate complement-mediated bacteriolysis of *S. flexneri* 3a. L-ABA is the average of

three biological replicates each performed in duplicate. p-values were calculated on $\log IC_{50}$ values by repeated measure Anova with Dunnett's correction for multiple comparisons. (B) OPA assay measures the percent of THP-1 cells that have phagocytosed *S. flexneri* 3a that was opsonized with 30 nM of the indicated mAb. This experiment is the result of five biological replicates each performed in duplicate, and p-values were calculated by repeated measure ANOVA with Dunnett's correction for multiple comparisons. Error bars represent standard deviation. (C) Invasion assay shows the percent invasion of *S. flexneri* 3a incubated with 1μM of the indicated mAb normalized to the invasion rate of *S. flexneri* 3a in PBS. This experiment is the result of four biological replicates each performed in duplicate, and p-values were calculated by repeated measure ANOVA with Dunnett's correction for multiple comparisons. Errors bars represent standard error of the mean (S.E.M.). For all plots, p values < 0.5 are denoted by a *.

Fig 6: Binding and functional analysis of hFlex3a2_v2 variants against *S. flexneri* 3b. (A) Schematic depicting the O-Ag structures of our panel of *S. flexneri* serotypes. (B) Surface staining with 50 nM of hFlex3a2_v2 variants and a non-binding control mAb to a panel of *S. flexneri* and *S. sonnei* serotypes. This experiment is the average of two replicates. (C) Binding curves from a titration ELISA against *S. flexneri* 3b OMVs (2.5 μg/mL) show relative binding potency of the parent mAb (red), single amino acid variants (green), and combinatorial variants (blue). ELISA binding curves are the average of two replicates. (D) L-ABA assay comparing the ability of hFlex3a2_v2, L33N, and S30G + L33N to coordinate complement-mediated bacteriolysis of *S. flexneri* 3b. L-ABA is the average of four biological replicates each performed in duplicate. (E) OPA assay measures the percent of THP-1 cells that have phagocytosed *S. flexneri* 3b that was opsonized with 30 nM of the indicated mAb. This experiment is the result of five biological replicates each performed in duplicate, and p-values were calculated by repeated measure ANOVA with Dunnett's correction for multiple comparisons. Error bars represent standard deviation. (F) Invasion assay shows the percent invasion of *S. flexneri* 3b incubated with 1μM of the indicated mAb normalized to the invasion rate of *S. flexneri* 3b in PBS. This experiment is the result of four biological replicates each performed in duplicate. Error bars represent standard error of the mean (S.E.M.). for all plots, p values < 0.5 are denoted by a *.

Fig S1: **Mutation enrichment in the VH library after panning.** (A) Fold-change in the frequency of next-generation sequencing reads for variant mutations at each VH site of hFlex3a2_v2 after two rounds of panning, relative to their frequency in the input library. (B) log10 enrichment of variants in the VH library after two rounds of panning against *S. flexneri* 3a and *S. sonnei*. Dotted line is 20 standard deviations above the mean mutation enrichment in the input library and indicates a stringent threshold set to distinguish bacteria-mediated enrichment from background variability.

Fig S2: Distribution of next-generation sequencing reads across the VL library variants after panning. A heatmap showing the percentage of all reads belonging to the indicated hFlex3a2_v2 variant after two rounds of panning against *S. flexneri* 3a.

Fig S3: Enrichment of VL mutations for increased affinity to the surface of *S. flexneri 3a* after two rounds of panning. Enrichment of the indicated amino acids in the library variants after panning against *S. flexneri* 3a was calculated relative to the enrichment against *S. sonnei*. All data is log10 transformed. White squares with an "X" through them indicate variants for which no reads were detected in either the input or output libraries, suggesting that these variants may not have been successfully synthesized.

Fig S4: hFlex3a2_v2 variant *S. flexneri* 3a OMV and polyreactiviy ELISAs (A) The same ELISA as Figure 4B is reproduced here, but with all variants labeled. (B) ELISA measuring non-specific binding of hFlex3a2_v2 variants to 5 μg/mL of insulin, CHO-SMPs, or ssDNA. A known poly-reactive mAb (4E10 targeting HIV-1) and a known non-polyreactive mAb (Adalimumab) serve as positive and negative controls, respectively. This experiment is the result of three replicates. (C) Gating strategy for quantifying OPA. Cells are gated first by size, then by CD45+ Dead- populations. An unrelated, nonbinding mAb negative control is used to determine the %CTV+ gate.

Fig S5: L-ABA analysis of hFlex3a2_v2 variants against *S. flexneri* 3a (A) L-ABA from Fig 5A is reproduced here, but with all variants labeled. (B) log10 IC_{50} from L-ABA and EC_{50} from ELISA are correlated. R^2 represents Pearson correlation coefficient.

Fig S6: hFlex3a2_v2 variant ELISA against *S. flexneri* 3b OMVs. (A) SDS-PAGE of crude LPS extract from *S. flexneri* 3a and *S. flexneri* 3a waaL::kan (O-Ag-) confirms that knocking out waaL eliminates O-Ag expression. Gel was stained with Pro-Q Emerald 3000. (B)The ELISA from Fig 6C is reproduced here, but with all variants labeled.

Acknowledgements

The hFlex3a2 mAb was generated by the laboratory of Dr. Moon Nahm at the University of Alabama Birmingham in collaboration with the Walter Reed Army Institute of Research (36). We thank collaborators from the Wisconsin National Primate Research Center, Jennifer Hayes, Dr. Faye Hartmann, and Dr. Eric Peterson, for sharing isolates WS-016 and WS-037. We thank Finora Franck for invaluable program management support, and we thank Katherine McKenney for assistance with 10X sequencing, and Mark Ochoa for assistance with cell culture. We also thank Dr. Stephen Baker and Dr. Timothy Scott for scientific advice and support, as well as providing the Shigella sonnei 53G lvp::kan strain. Finally, we would like to thank current and former members of the RESISTANT Research Steering Group (including Wellcome Trust Program Officers) for their invaluable support of this work, including Dr. Pete Gardner, Dr. Colleen Loynachan, Dr. Kate Mills, Dr. Nathalie Herze-Vourc'h, and Dr. Christiane Gerke. This work was supported by the Wellcome Trust RESISTANT grant.

Works Cited:

1. GBD 2021 Antimicrobial Resistance Collaborators. Global burden of bacterial antimicrobial resistance 1990-2021: a systematic analysis with forecasts to 2050. Lancet Lond Engl. 2024 Sept 28;404(10459):1199–226.

828 2. La Guidara C, Adamo R, Sala C, Micoli F. Vaccines and Monoclonal Antibodies as
829 Alternative Strategies to Antibiotics to Fight Antimicrobial Resistance. Int J Mol Sci. 2024
830 May 17;25(10):5487.

831 3. Perrett KP, Nolan TM, McVernon J. A Licensed Combined Haemophilus influenzae Type b-
832 Serogroups C and Y Meningococcal Conjugate Vaccine. Infect Dis Ther. 2013 June;2(1):1–
833 13.

834 4. Ladhani SN. Two decades of experience with the Haemophilus influenzae serotype b
835 conjugate vaccine in the United Kingdom. Clin Ther. 2012 Feb;34(2):385–99.

836 5. Hedari CP, Khinkarly RW, Dbaibo GS. Meningococcal serogroups A, C, W-135, and Y
837 tetanus toxoid conjugate vaccine: a new conjugate vaccine against invasive meningococcal
838 disease. Infect Drug Resist. 2014;7:85–99.

839 6. Grijalva CG, Nuorti JP, Arbogast PG, Martin SW, Edwards KM, Griffin MR. Decline in
840 pneumonia admissions after routine childhood immunisation with pneumococcal conjugate
841 vaccine in the USA: a time-series analysis. Lancet Lond Engl. 2007 Apr 7;369(9568):1179–
842 86.

843 7. Milligan R, Paul M, Richardson M, Neuberger A. Vaccines for preventing typhoid fever.
844 Cochrane Database Syst Rev. 2018 May 31;5(5):CD001261.

845 8. Baker S, Krishna A, Higham S, Naydenova P, O'Leary S, Scott JB, et al. Exploiting human
846 immune repertoire transgenic mice for protective monoclonal antibodies against
847 antimicrobial resistant Acinetobacter baumannii. Nat Commun. 2024 Sept 12;15(1):7979.

848 9. Aguiar-Alves F, Le HN, Tran VG, Gras E, Vu TTT, Dong OX, et al. Antivirulence
849 Bispecific Monoclonal Antibody-Mediated Protection against Pseudomonas aeruginosa
850 Ventilator-Associated Pneumonia in a Rabbit Model. Antimicrob Agents Chemother. 2022
851 Feb 15;66(2):e0202221.

852 10. Nielsen TB, Yan J, Slarve M, Lu P, Li R, Ruiz J, et al. Monoclonal Antibody Therapy
853 against Acinetobacter baumannii. Infect Immun. 2021 Sept 16;89(10):e0016221.

854 11. Nielsen TB, Yan J, Luna BM, Talyansky Y, Slarve M, Bonomo RA, et al. Monoclonal
855 Antibody Requires Immunomodulation for Efficacy Against Acinetobacter baumannii
856 Infection. J Infect Dis. 2021 Dec 15;224(12):2133–47.

857 12. Richards AF, Doering JE, Lozito SA, Varrone JJ, Willsey GG, Pauly M, et al. Inhibition of
858 invasive salmonella by orally administered IgA and IgG monoclonal antibodies. PLoS Negl
859 Trop Dis. 2020 Mar;14(3):e0007803.

860 13. Gulati S, Beurskens FJ, de Kreuk BJ, Roza M, Zheng B, DeOliveira RB, et al. Complement
861 alone drives efficacy of a chimeric antigonococcal monoclonal antibody. PLoS Biol. 2019
862 June;17(6):e3000323.

863 14. Kalfopoulou E, Laverde D, Miklic K, Romero-Saavedra F, Malic S, Carboni F, et al.
864 Development of Opsonic Mouse Monoclonal Antibodies against Multidrug-Resistant
865 Enterococci. Infect Immun. 2019 Sept;87(9):e00276-19.

866 15. Pennini ME, De Marco A, Pelletier M, Bonnell J, Cvitkovic R, Beltramello M, et al. Immune
867 stealth-driven O2 serotype prevalence and potential for therapeutic antibodies against
868 multidrug resistant Klebsiella pneumoniae. Nat Commun. 2017 Dec 8;8(1):1991.

869 16. Rollenske T, Szijarto V, Lukasiewicz J, Guachalla LM, Stojkovic K, Hartl K, et al. Cross-
870 specificity of protective human antibodies against Klebsiella pneumoniae LPS O-antigen.
871 Nat Immunol. 2018 June;19(6):617–24.

872 17. Parzych EM, Gulati S, Zheng B, Bah MA, Elliott STC, Chu JD, et al. Synthetic DNA
873 Delivery of an Optimized and Engineered Monoclonal Antibody Provides Rapid and
874 Prolonged Protection against Experimental Gonococcal Infection. mBio. 2021 Mar
875 16;12(2):e00242-21.

876 18. Que YA, Lazar H, Wolff M, François B, Laterre PF, Mercier E, et al. Assessment of
877 panobacumab as adjunctive immunotherapy for the treatment of nosocomial Pseudomonas
878 aeruginosa pneumonia. Eur J Clin Microbiol Infect Dis Off Publ Eur Soc Clin Microbiol.
879 2014 Oct;33(10):1861–7.

880 19. Chastre J, François B, Bourgeois M, Komnos A, Ferrer R, Rahav G, et al. Safety, efficacy,
881 and pharmacokinetics of gremubamab (MEDI3902), an anti-Pseudomonas aeruginosa
882 bispecific human monoclonal antibody, in P. aeruginosa-colonised, mechanically ventilated
883 intensive care unit patients: a randomised controlled trial. Crit Care Lond Engl. 2022 Nov
884 15;26(1):355.

885 20. Healthcare G. ATS 2025: promising results with gremubamab in bronchiectasis [Internet].
886 Clinical Trials Arena. 2025 [cited 2025 Sept 8]. Available from:
887 https://www.clinicaltrialsarena.com/analyst-comment/ats-2025-promising-results-
888 gremubamab-bronchiectasis/

889 21. Erridge C, Bennett-Guerrero E, Poxton IR. Structure and function of lipopolysaccharides.
890 Microbes Infect. 2002 July;4(8):837–51.

891 22. Formal SB, Oaks EV, Olsen RE, Wingfield-Eggleston M, Snoy PJ, Cogan JP. Effect of prior
892 infection with virulent Shigella flexneri 2a on the resistance of monkeys to subsequent
893 infection with Shigella sonnei. J Infect Dis. 1991 Sept;164(3):533–7.

894 23. Cohen D, Meron-Sudai S, Bialik A, Asato V, Goren S, Ariel-Cohen O, et al. Serum IgG
895 antibodies to Shigella lipopolysaccharide antigens - a correlate of protection against
896 shigellosis. Hum Vaccines Immunother. 2019;15(6):1401–8.

897 24. Kappler K, Hennet T. Emergence and significance of carbohydrate-specific antibodies.
898 Genes Immun. 2020 Aug;21(4):224–39.

899 25. Haji-Ghassemi O, Blackler RJ, Martin Young N, Evans SV. Antibody recognition of
900 carbohydrate epitopes. Glycobiology. 2015 Sept;25(9):920–52.

901 26. Borenstein-Katz A, Warszawski S, Amon R, Eilon M, Cohen-Dvashi H, Leviatan Ben-Arye
902 S, et al. Biomolecular Recognition of the Glycan Neoantigen CA19-9 by Distinct
903 Antibodies. J Mol Biol. 2021 July 23;433(15):167099.

904 27. Amon R, Rosenfeld R, Perlmutter S, Grant OC, Yehuda S, Borenstein-Katz A, et al. Directed
905 Evolution of Therapeutic Antibodies Targeting Glycosylation in Cancer. Cancers. 2020 Sept
906 30;12(10):2824.

907 28. Haji-Ghassemi O, Müller-Loennies S, Brooks CL, MacKenzie CR, Caveney N, Van
908 Petegem F, et al. Subtle Changes in the Combining Site of the Chlamydiaceae-Specific mAb
909 S25-23 Increase the Antibody-Carbohydrate Binding Affinity by an Order of Magnitude.
910 Biochemistry. 2019 Feb 12;58(6):714–26.

911 29. Hu J, Huang X, Ling CC, Bundle DR, Cheung NKV. Reducing epitope spread during
912 affinity maturation of an anti-ganglioside GD2 antibody. J Immunol Baltim Md 1950. 2009
913 Nov 1;183(9):5748–55.

914 30. Thomas R, Patenaude SI, MacKenzie CR, To R, Hirama T, Young NM, et al. Structure of an
915 anti-blood group A Fv and improvement of its binding affinity without loss of specificity. J
916 Biol Chem. 2002 Jan 18;277(3):2059–64.

917 31. Brorson K, Thompson C, Wei G, Krasnokutsky M, Stein KE. Mutational analysis of avidity
918 and fine specificity of anti-levan antibodies. J Immunol Baltim Md 1950. 1999 Dec
919 15;163(12):6694–701.

920 32. Deng SJ, MacKenzie CR, Sadowska J, Michniewicz J, Young NM, Bundle DR, et al.
921 Selection of antibody single-chain variable fragments with improved carbohydrate binding
922 by phage display. J Biol Chem. 1994 Apr 1;269(13):9533–8.

923 33. Brummell DA, Sharma VP, Anand NN, Bilous D, Dubuc G, Michniewicz J, et al. Probing
924 the combining site of an anti-carbohydrate antibody by saturation-mutagenesis: role of the
925 heavy-chain CDR3 residues. Biochemistry. 1993 Feb 2;32(4):1180–7.

926 34. Yelton DE, Rosok MJ, Cruz G, Cosand WL, Bajorath J, Hellström I, et al. Affinity
927 maturation of the BR96 anti-carcinoma antibody by codon-based mutagenesis. J Immunol
928 Baltim Md 1950. 1995 Aug 15;155(4):1994–2004.

929 35. Wang W, Bunyatov M, Moffat D, Lopez-Barbosa N, DeLisa MP. Engineering affinity-
930 matured variants of an anti-polysialic acid monoclonal antibody with superior cytotoxicity-
931 mediating potency. Cell Chem Biol. 2025 Aug 21;32(8):1042-1057.e6.

932 36. Deng SJ, MacKenzie CR, Hirama T, Brousseau R, Lowary TL, Young NM, et al. Basis for
933 selection of improved carbohydrate-binding single-chain antibodies from synthetic gene
934 libraries. Proc Natl Acad Sci U S A. 1995 May 23;92(11):4992–6.

935 37. Lin J, Smith MA, Benjamin WH, Kaminski RW, Wenzel H, Nahm MH. Monoclonal
936 Antibodies to Shigella Lipopolysaccharide Are Useful for Vaccine Production. Clin Vaccine
937 Immunol CVI. 2016 Aug;23(8):681–8.

938 38. Mancini F, Gasperini G, Rossi O, Aruta MG, Raso MM, Alfini R, et al. Dissecting the
939 contribution of O-Antigen and proteins to the immunogenicity of Shigella sonnei generalized
940 modules for membrane antigens (GMMA). Sci Rep. 2021 Jan 13;11(1):906.

941 39. Kang TH, Seong BL. Solubility, Stability, and Avidity of Recombinant Antibody Fragments
942 Expressed in Microorganisms. Front Microbiol. 2020;11:1927.

943 40. Maynard JA, Maassen CBM, Leppla SH, Brasky K, Patterson JL, Iverson BL, et al.
944 Protection against anthrax toxin by recombinant antibody fragments correlates with antigen
945 affinity. Nat Biotechnol. 2002 June;20(6):597–601.

946 41. Chowdhury PS, Vasmatzis G. Engineering scFvs for improved stability. Methods Mol Biol
947 Clifton NJ. 2003;207:237–54.

948 42. Berry SK, Rust S, Caceres C, Irving L, Bartholdson Scott J, Tabor DE, et al. Phenotypic
949 whole-cell screening identifies a protective carbohydrate epitope on Klebsiella pneumoniae.
950 mAbs. 2022;14(1):2006123.

951 43. Perepelov AV, Shekht ME, Liu B, Shevelev SD, Ledov VA, Senchenkova SN, et al. Shigella
952 flexneri O-antigens revisited: final elucidation of the O-acetylation profiles and a survey of
953 the O-antigen structure diversity. FEMS Immunol Med Microbiol. 2012 Nov;66(2):201–10.

954 44. Doepker LE, Danon S, Harkins E, Ralph DK, Yaffe Z, Garrett ME, et al. Development of
955 antibody-dependent cell cytotoxicity function in HIV-1 antibodies. eLife. 2021 Jan
956 11;10:e63444.

957 45. Swindells MB, Porter CT, Couch M, Hurst J, Abhinandan KR, Nielsen JH, et al. abYsis:
958 Integrated Antibody Sequence and Structure-Management, Analysis, and Prediction. J Mol
959 Biol. 2017 Feb 3;429(3):356–64.

960 46. Brochet X, Lefranc MP, Giudicelli V. IMGT/V-QUEST: the highly customized and
961 integrated system for IG and TR standardized V-J and V-D-J sequence analysis. Nucleic
962 Acids Res. 2008 July 1;36(Web Server issue):W503-508.

963 47. Ye J, Ma N, Madden TL, Ostell JM. IgBLAST: an immunoglobulin variable domain
964 sequence analysis tool. Nucleic Acids Res. 2013 July;41(Web Server issue):W34-40.

965 48. Berlanda Scorza F, Colucci AM, Maggiore L, Sanzone S, Rossi O, Ferlenghi I, et al. High
966 yield production process for Shigella outer membrane particles. PloS One.
967 2012;7(6):e35616.

968 49. Han W, Wu B, Li L, Zhao G, Woodward R, Pettit N, et al. Defining function of
969 lipopolysaccharide O-antigen ligase WaaL using chemoenzymatically synthesized substrates.
970 J Biol Chem. 2012 Feb 17;287(8):5357–65.

971 50. Herring CD, Glasner JD, Blattner FR. Gene replacement without selection: regulated
972 suppression of amber mutations in Escherichia coli. Gene. 2003 June 5;311:153–63.

973 51. Heckman KL, Pease LR. Gene splicing and mutagenesis by PCR-driven overlap extension.
974 Nat Protoc. 2007;2(4):924–32.

975 52. Andris-Widhopf J, Rader C, Steinberger P, Fuller R, Barbas CF. Methods for the generation
976 of chicken monoclonal antibody fragments by phage display. J Immunol Methods. 2000 Aug
977 28;242(1–2):159–81.

978 53. Silva RP, DiVenere AM, Amengor D, Maynard JA. Antibodies binding diverse pertactin
979 epitopes protect mice from Bordetella pertussis infection. J Biol Chem. 2022
980 Mar;298(3):101715.

981 54. Cai H, Yao H, Li T, Hutter CAJ, Li Y, Tang Y, et al. An improved fluorescent tag and its
982 nanobodies for membrane protein expression, stability assay, and purification. Commun
983 Biol. 2020 Dec 10;3(1):753.

984 55. Micoli F, Rondini S, Gavini M, Pisoni I, Lanzilao L, Colucci AM, et al. A scalable method
985 for O-antigen purification applied to various Salmonella serovars. Anal Biochem. 2013 Mar
986 1;434(1):136–45.

987 56. Caradonna V, Pinto M, Alfini R, Giannelli C, Iturriza M, Micoli F, et al. High-Throughput
988 Luminescence-Based Serum Bactericidal Assay Optimization and Characterization to Assess
989 Human Sera Functionality Against Multiple Shigella flexneri Serotypes. Int J Mol Sci. 2024
990 Oct 16;25(20):11123.

991 57. Weinblatt ME, Keystone EC, Furst DE, Moreland LW, Weisman MH, Birbara CA, et al.
992 Adalimumab, a fully human anti-tumor necrosis factor alpha monoclonal antibody, for the
993 treatment of rheumatoid arthritis in patients taking concomitant methotrexate: the ARMADA
994 trial. Arthritis Rheum. 2003 Jan;48(1):35–45.

995 58. Elsinghorst EA. Measurement of invasion by gentamicin resistance. Methods Enzymol.
996 1994;236:405–20.

997 59. Darveau RP, Hancock RE. Procedure for isolation of bacterial lipopolysaccharides from both
998 smooth and rough Pseudomonas aeruginosa and Salmonella typhimurium strains. J Bacteriol.
999 1983 Aug;155(2):831–8.

1000

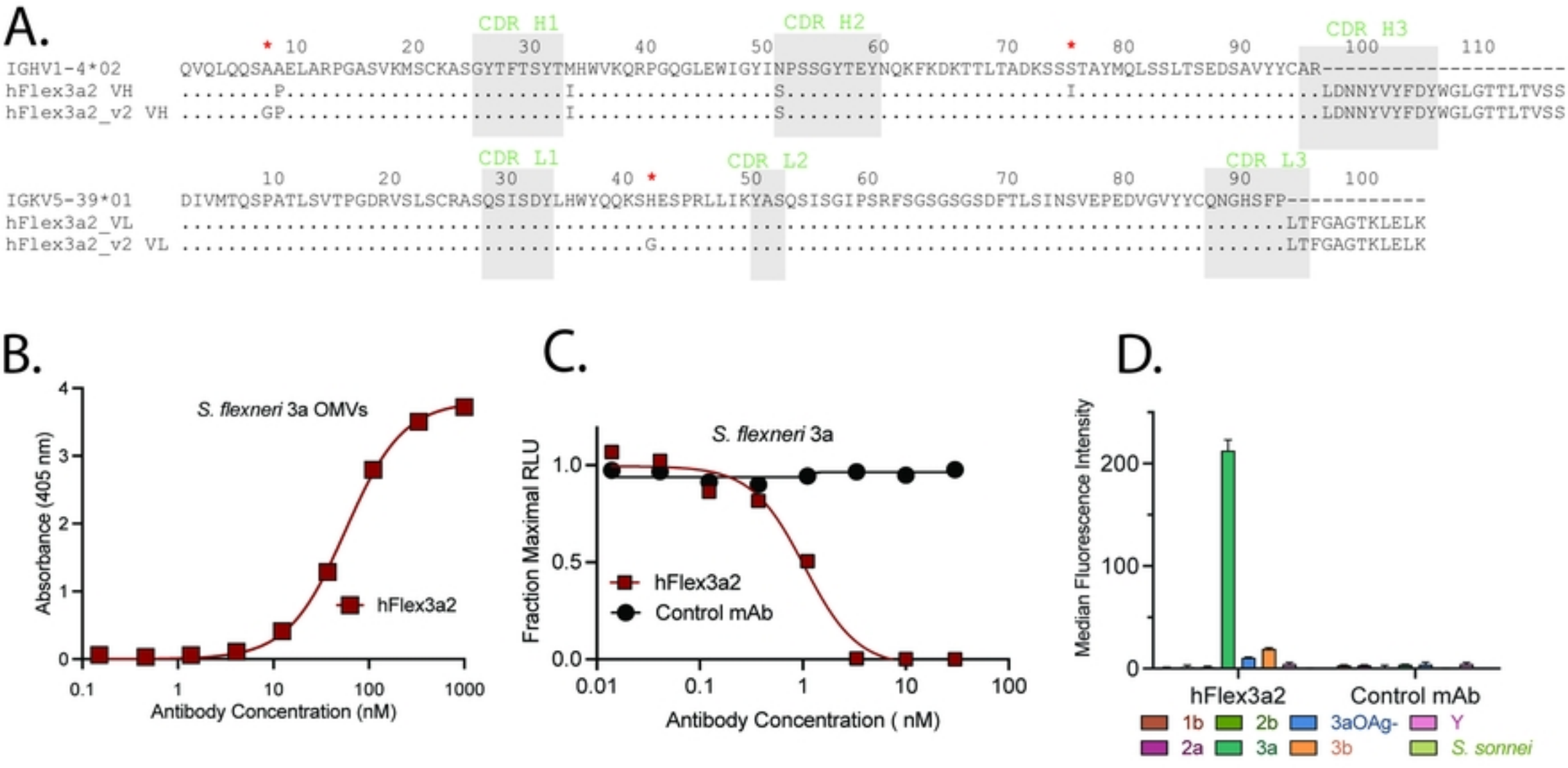
A.
CDR H1
CDR H2
CDR H3
* 10 20 30 40 50 60 70 * 80 90 100 110
IGHV1-4*02 QVQLQQSAAELARPGASVKMSCKASGYTFTSYTMHWVKQRPGQGLEWIGYINPSSGYTEYNQKFKDKTTLTADKSSSTAYMQLSSLTSEDSAVYYCAR----------
hFlex3a2 VH .....P.....I.....S.....I.....LDNNYVYFDYWGLGTTLTVSS
hFlex3a2_v2 VH .....GP.....I.....S.....LDNNYVYFDYWGLGTTLTVSS
CDR L1
CDR L2
CDR L3
10 20 30 40 * 50 60 70 80 90 100
IGKV5-39*01 DIVMTQSPATLSVTPGDRVSLSCRASQSISDYLHWYQQKSHESPRLLIKYASQSISGIPSRFSGSGSGSDFTLSINSVEPEDVGVYYCQNGHSFP----------
hFlex3a2_VL .....LTFGAGTKLELK
hFlex3a2_v2 VL .....G.....LTFGAGTKLELK
B.
S. flexneri 3a OMVs
Absorbance (405 nm)
hFlex3a2
Antibody Concentration (nM)
C.
S. flexneri 3a
Fraction Maximal RLU
hFlex3a2
Control mAb
Antibody Concentration (nM)
D.
Median Fluorescence Intensity
hFlex3a2
Control mAb
1b
2b
3aOAg-
Y
2a
3a
3b
S. sonnei

Figure 1

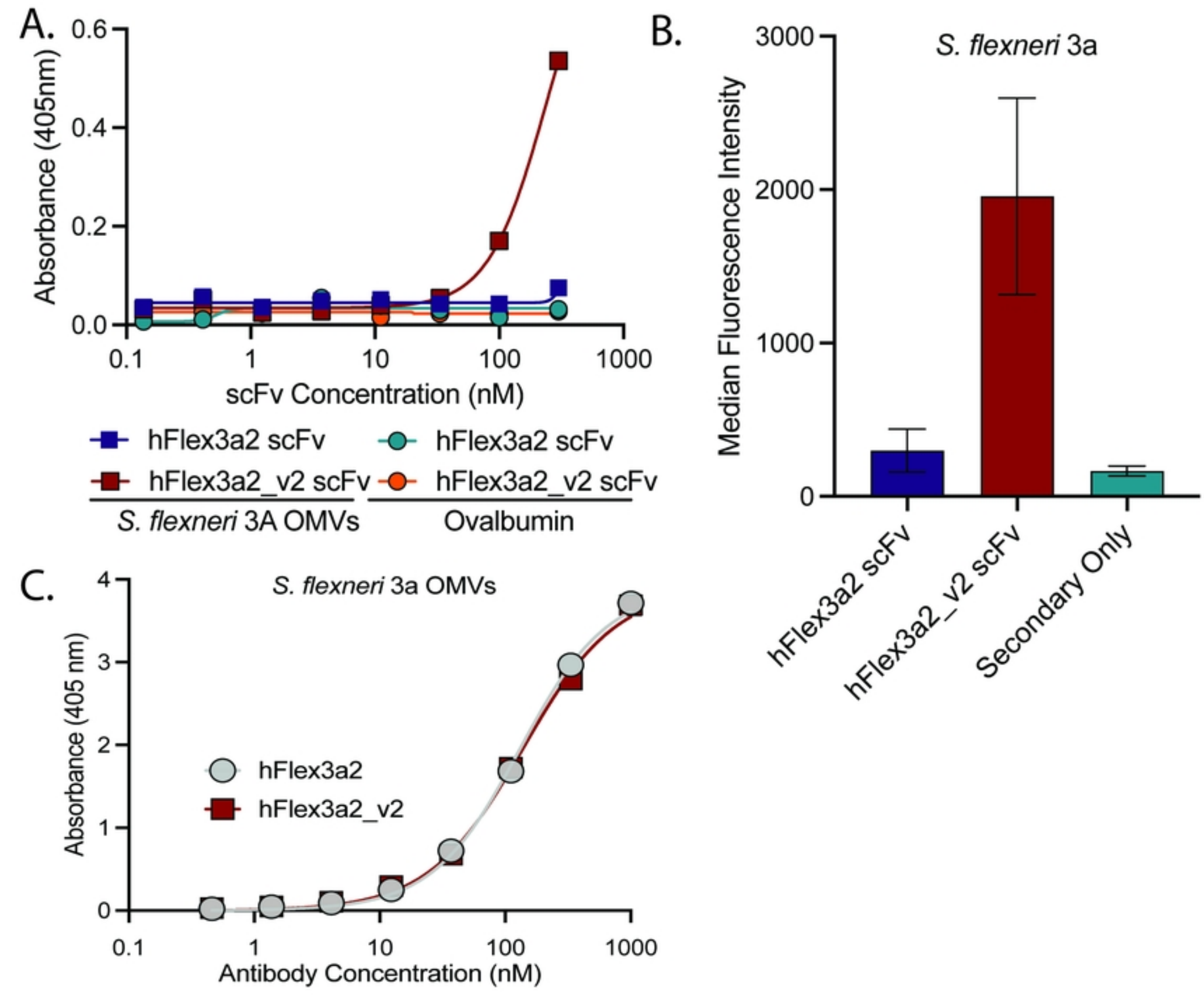
A.
Absorbance (405nm)
0.6
0.4
0.2
0.0
0.1
1
10
100
1000
scFv Concentration (nM)
hFlex3a2 scFv
hFlex3a2_v2 scFv
hFlex3a2 scFv
hFlex3a2_v2 scFv
S. flexneri 3A OMVs
Ovalbumin
B.
S. flexneri 3a
Median Fluorescence Intensity
3000
2000
1000
0
hFlex3a2 scFv
hFlex3a2_v2 scFv
Secondary Only
C.
S. flexneri 3a OMVs
Absorbance (405 nm)
4
3
2
1
0
hFlex3a2
hFlex3a2_v2
0.1
1
10
100
1000
Antibody Concentration (nM)

Figure 2

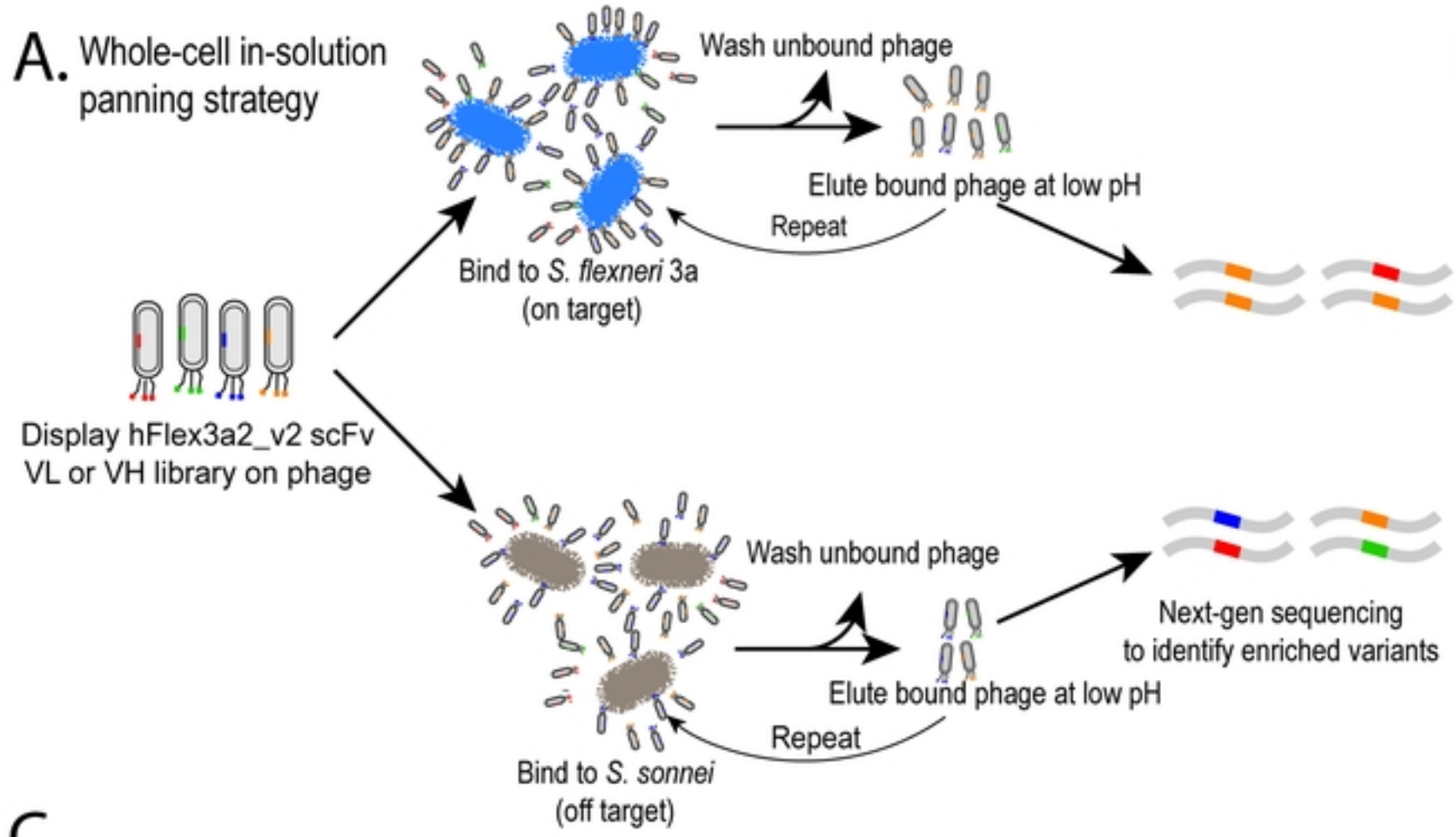
A.
Whole-cell in-solution panning strategy
Wash unbound phage
Elute bound phage at low pH
Repeat
Bind to S. flexneri 3a (on target)
Display hFlex3a2_v2 scFv VL or VH library on phage
Wash unbound phage
Elute bound phage at low pH
Repeat
Bind to S. sonnei (off target)
Next-gen sequencing to identify enriched variants

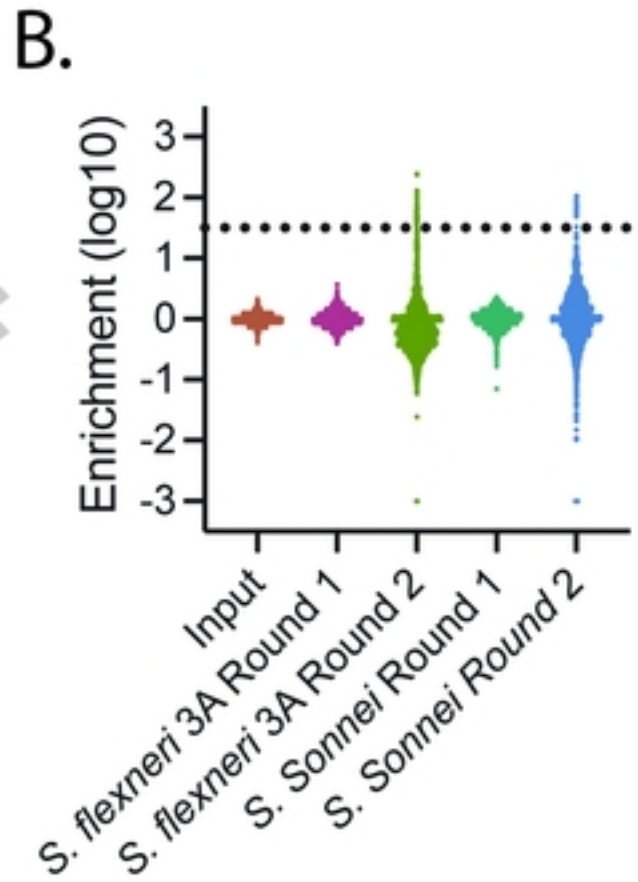
B.
Enrichment (log10)
3
2
1
0
-1
-2
-3
Input
S. flexneri 3A Round 1
S. flexneri 3A Round 2
S. Sonnei Round 1
S. Sonnei Round 2

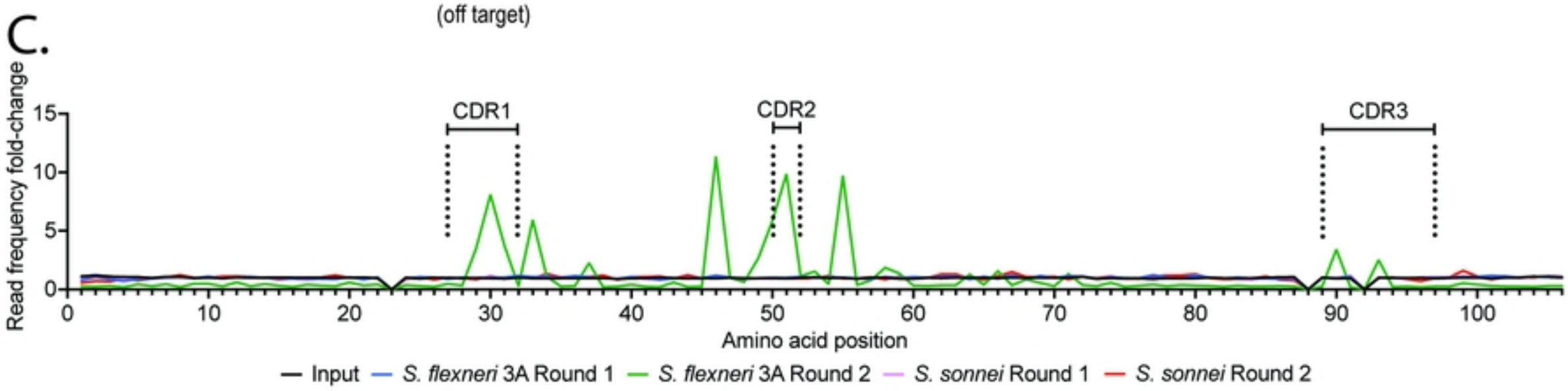
C.
Read frequency fold-change
15
10
5
0
CDR1
CDR2
CDR3
0
10
20
30
40
50
60
70
80
90
100
Amino acid position
Input
S. flexneri 3A Round 1
S. flexneri 3A Round 2
S. sonnei Round 1
S. sonnei Round 2

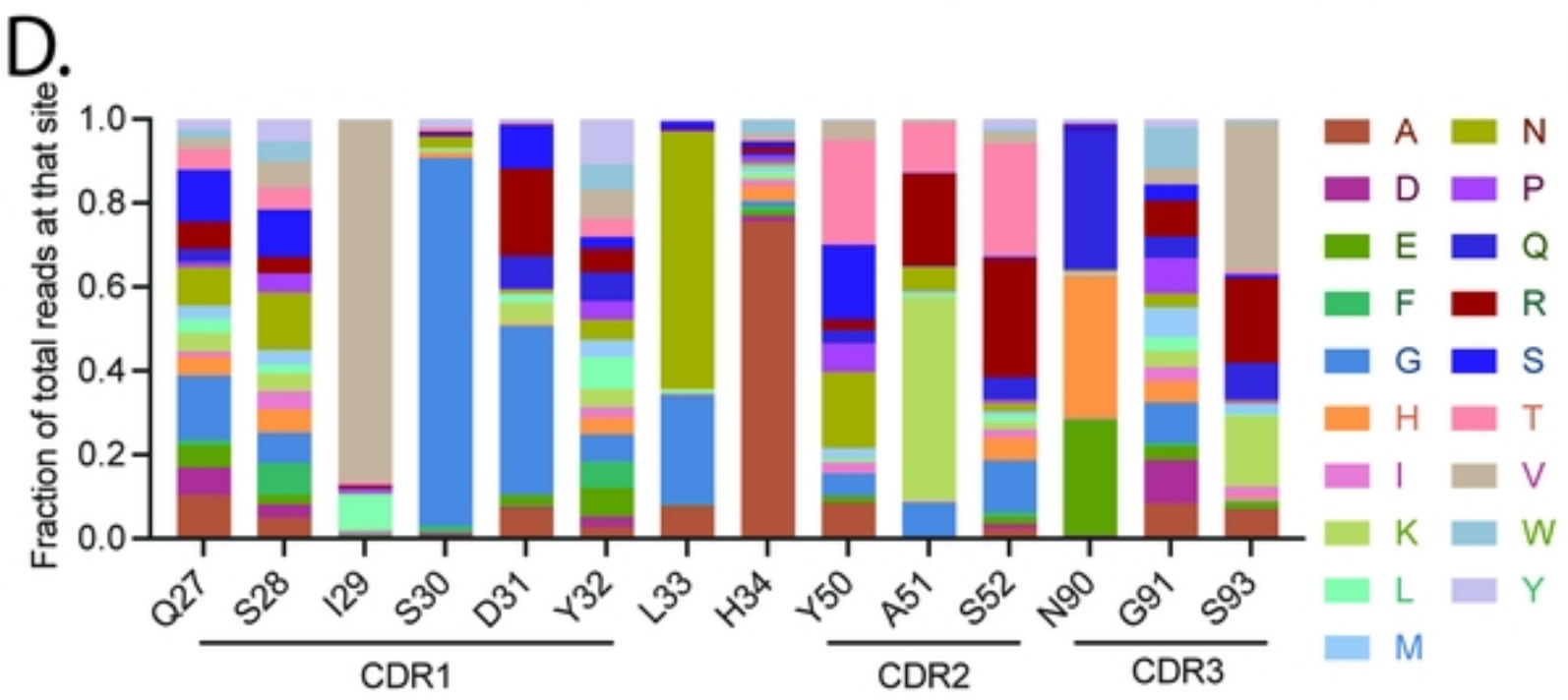
D.
Fraction of total reads at that site
1.0
0.8
0.6
0.4
0.2
0.0
Q27
S28
I29
S30
D31
Y32
L33
H34
Y50
A51
S52
N90
G91
S93
CDR1
CDR2
CDR3
A
D
E
F
G
H
I
K
L
M
N
P
Q
R
S
T
V
W
Y

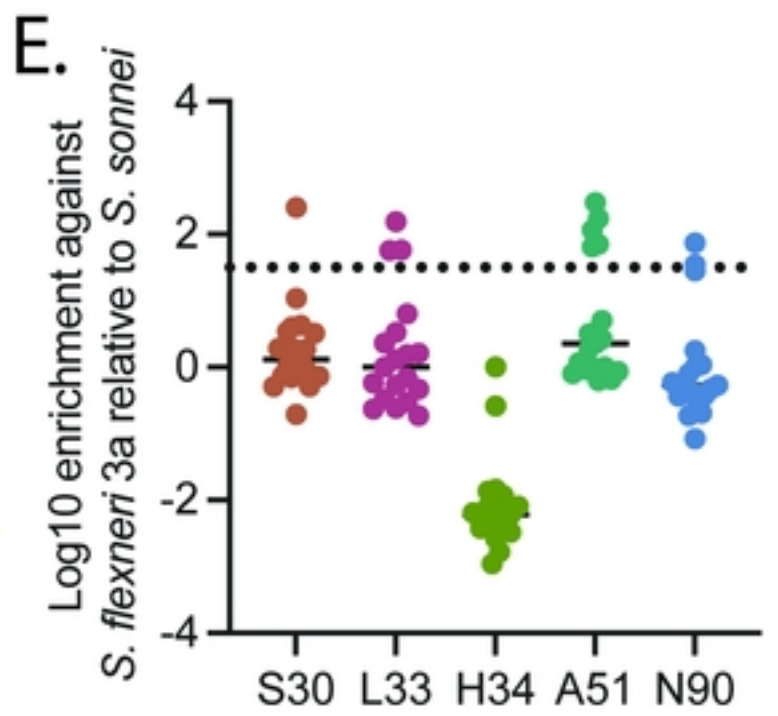
E.
Log10 enrichment against S. flexneri 3a relative to S. sonnei
4
2
0
-2
-4
S30
L33
H34
A51
N90

Figure 3

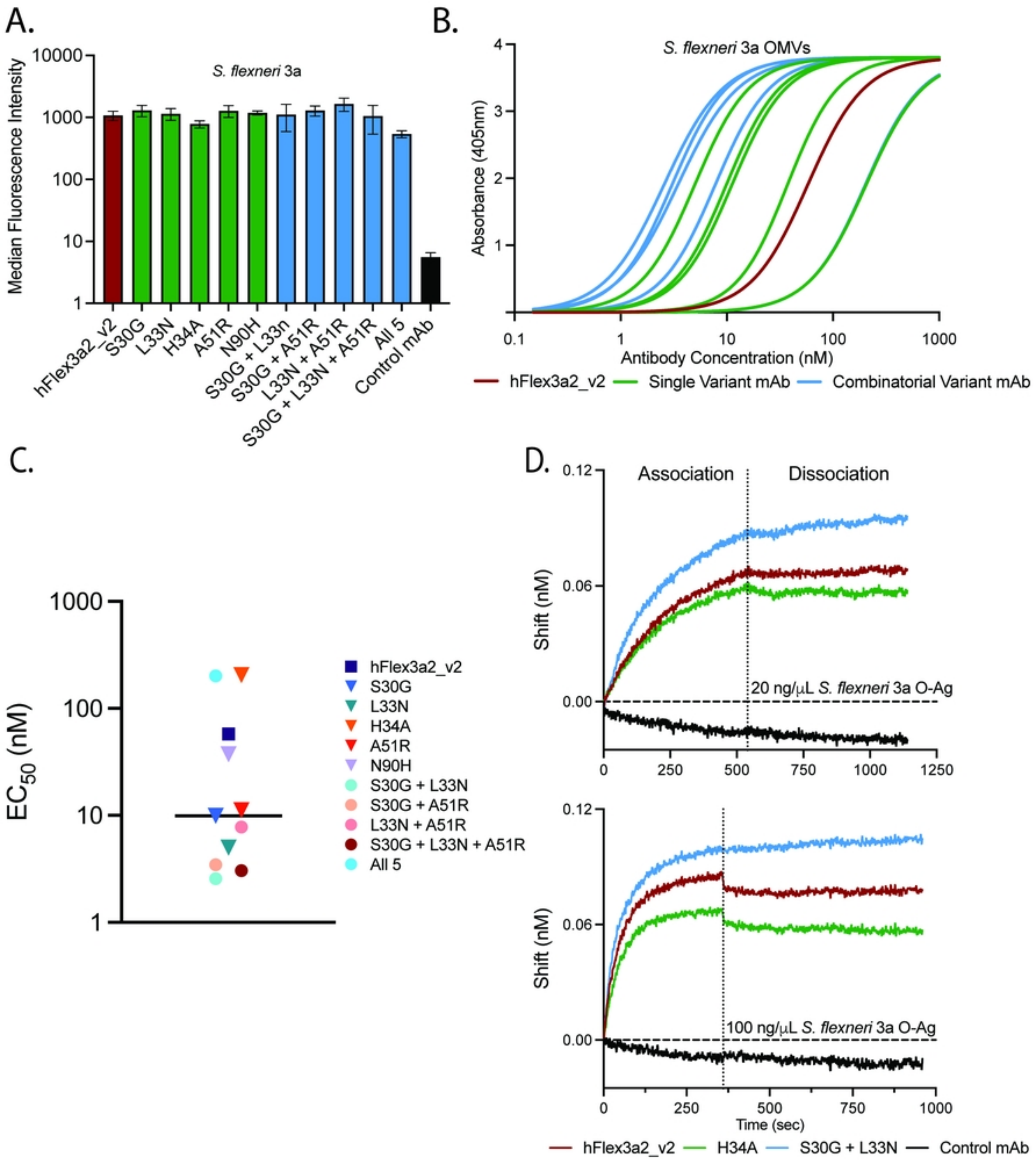
A.
S. flexneri 3a
Median Fluorescence Intensity
10000
1000
100
10
1
hFlex3a2_v2
S30G
L33N
H34A
A51R
N90H
S30G + L33n
S30G + A51R
L33N + A51R
S30G + L33N + A51R
All 5
Control mAb
B.
S. flexneri 3a OMVs
Absorbance (405nm)
4
3
2
1
0.1
1
10
100
1000
Antibody Concentration (nM)
hFlex3a2_v2
Single Variant mAb
Combinatorial Variant mAb
C.
EC50 (nM)
1000
100
10
1
hFlex3a2_v2
S30G
L33N
H34A
A51R
N90H
S30G + L33N
S30G + A51R
L33N + A51R
S30G + L33N + A51R
All 5
D.
Association
Dissociation
Shift (nM)
0.12
0.06
0.00
20 ng/µL S. flexneri 3a O-Ag
0
250
500
750
1000
1250
100 ng/µL S. flexneri 3a O-Ag
Time (sec)
hFlex3a2_v2
H34A
S30G + L33N
Control mAb

Figure 4

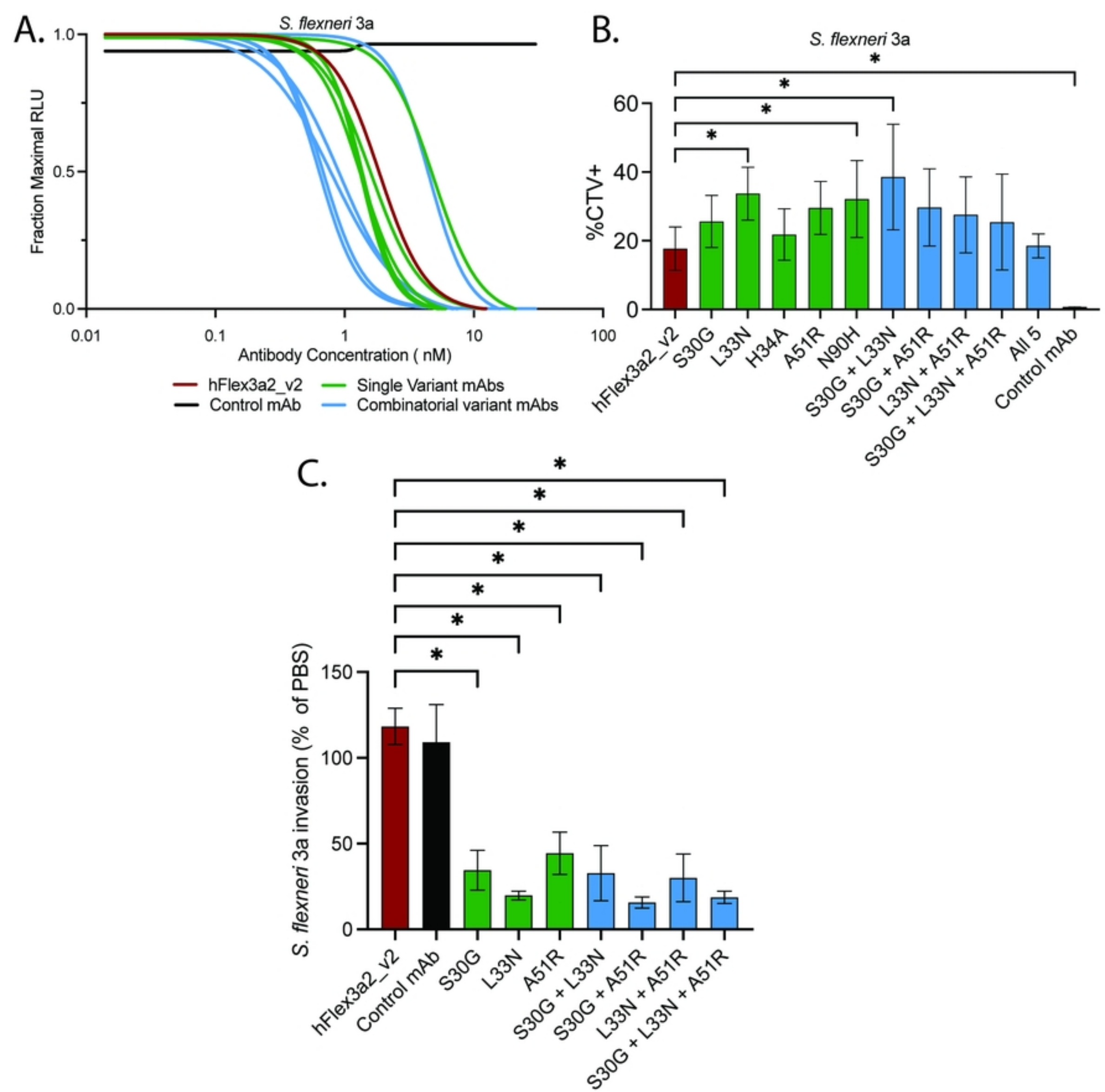
A.
S. flexneri 3a
Fraction Maximal RLU
1.0
0.5
0.0
0.01
0.1
1
10
100
Antibody Concentration (nM)
hFlex3a2_v2
Control mAb
Single Variant mAbs
Combinatorial variant mAbs
B.
S. flexneri 3a
%CTV+
60
40
20
0
*
hFlex3a2_v2
S30G
L33N
H34A
A51R
N90H
S30G + L33N
S30G + A51R
L33N + A51R
S30G + L33N + A51R
All 5
Control mAb
C.
S. flexneri 3a invasion (% of PBS)
150
100
50
0
*
hFlex3a2_v2
Control mAb
S30G
L33N
A51R
S30G + L33N
S30G + A51R
L33N + A51R
S30G + L33N + A51R

Figure 5

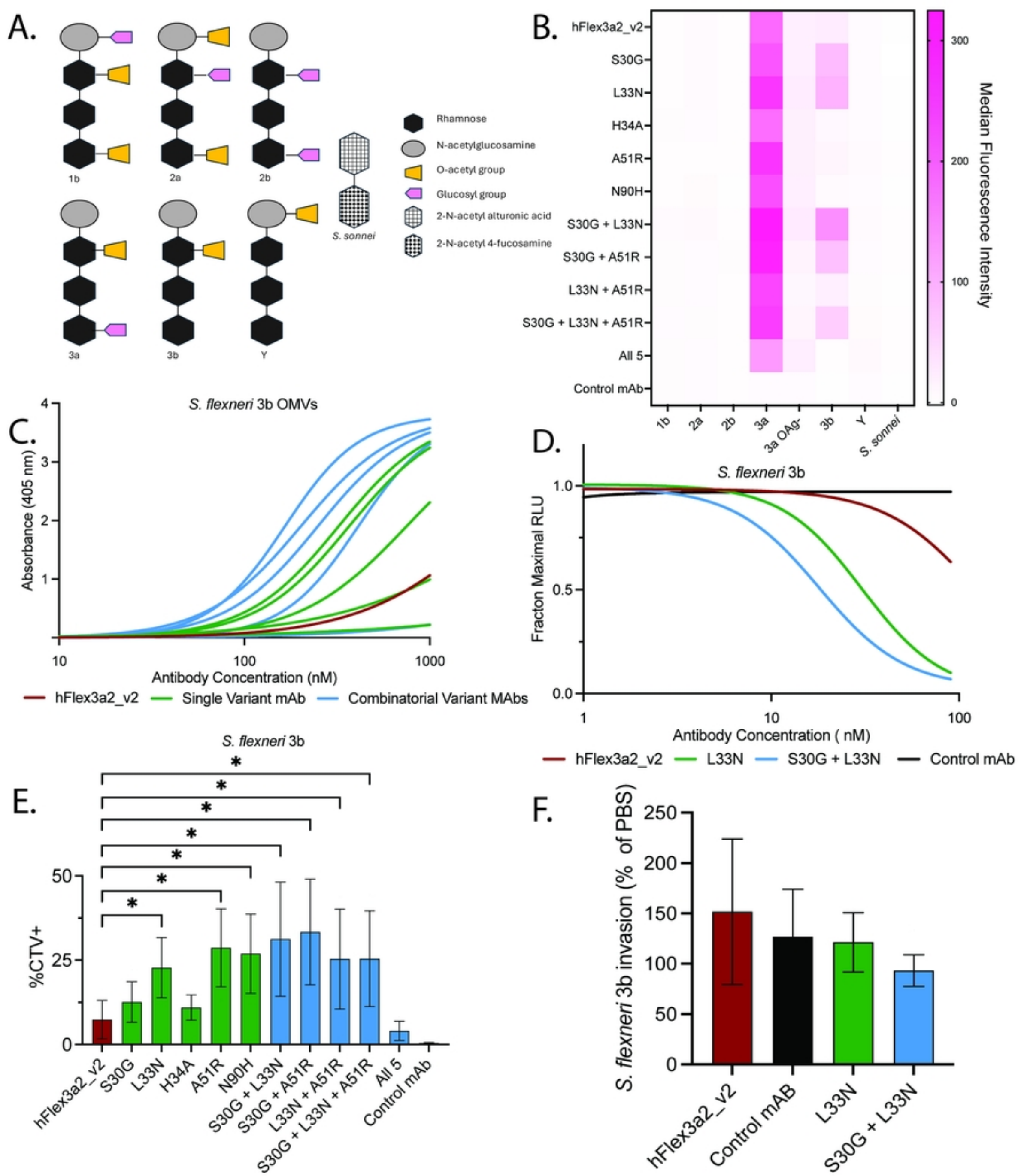
A.
1b
2a
2b
3a
3b
Y
S. sonnei
Rhamnose
N-acetylglucosamine
O-acetyl group
Glucosyl group
2-N-acetyl alturonic acid
2-N-acetyl 4-fucosamine
B.
hFlex3a2_v2
S30G
L33N
H34A
A51R
N90H
S30G + L33N
S30G + A51R
L33N + A51R
S30G + L33N + A51R
All 5
Control mAb
1b
2a
2b
3a
3a OAg-
3b
Y
S. sonnei
Median Fluorescence Intensity
300
200
100
0
C.
S. flexneri 3b OMVs
Absorbance (405 nm)
Antibody Concentration (nM)
hFlex3a2_v2
Single Variant mAb
Combinatorial Variant MAbs
D.
S. flexneri 3b
Fracton Maximal RLU
Antibody Concentration (nM)
hFlex3a2_v2
L33N
S30G + L33N
Control mAb
E.
S. flexneri 3b
%CTV+
hFlex3a2_v2
S30G
L33N
H34A
A51R
N90H
S30G + L33N
S30G + A51R
L33N + A51R
S30G + L33N + A51R
All 5
Control mAb
F.
S. flexneri 3b invasion (% of PBS)
hFlex3a2_v2
Control mAB
L33N
S30G + L33N

Figure 6

Antibody	3a fold enrichment	Sonnei fold enrichment	3a ELISA EC50 (nM)	3a L-ABA IC50 (nM)	3a OPA (%CTV+)	3a Invasion assay (% of PBS)	3b ELISA EC50 (nM)	3a L-ABA IC50 (nM)	3b OPA (%CTV+)	3b Invasion Assay (% of PBS)
hf lex3a2_v2	—	—	57.8	1.86	17.7	118.3	2,140	125.80	7.4	151.7
S30G	243.5	1.0	9.9	1.35	25.6	34.5	367	—	12.6	—
L33N	129.9	0.8	5.0	1.32	33.7	19.8	323	30.40	22.8	121.3
H34A	15.9	61.2	205.1	4.86	21.8	—	112,634	—	11.0	—
A51R	128.5	0.7	11.2	1.38	29.6	44.4	750	—	28.7	—
N90H	105.2	3.7	37.2	1.60	32.2	—	3,074	—	26.9	—
S30G + L33N	—	—	2.6	0.68	38.6	32.8	165	17.96	31.3	93.33
S30G + A51R	—	—	3.5	0.63	29.7	15.7	249	—	33.4	—
L33N + A51R	—	—	7.8	0.92	27.6	30.1	412	—	25.3	—
S30G + L33N + A51R	—	—	3.0	0.80	25.4	18.7	202	—	25.4	—
All 5	—	—	201.3	4.50	18.5	—	20,313	—	4.1	—

Table 1

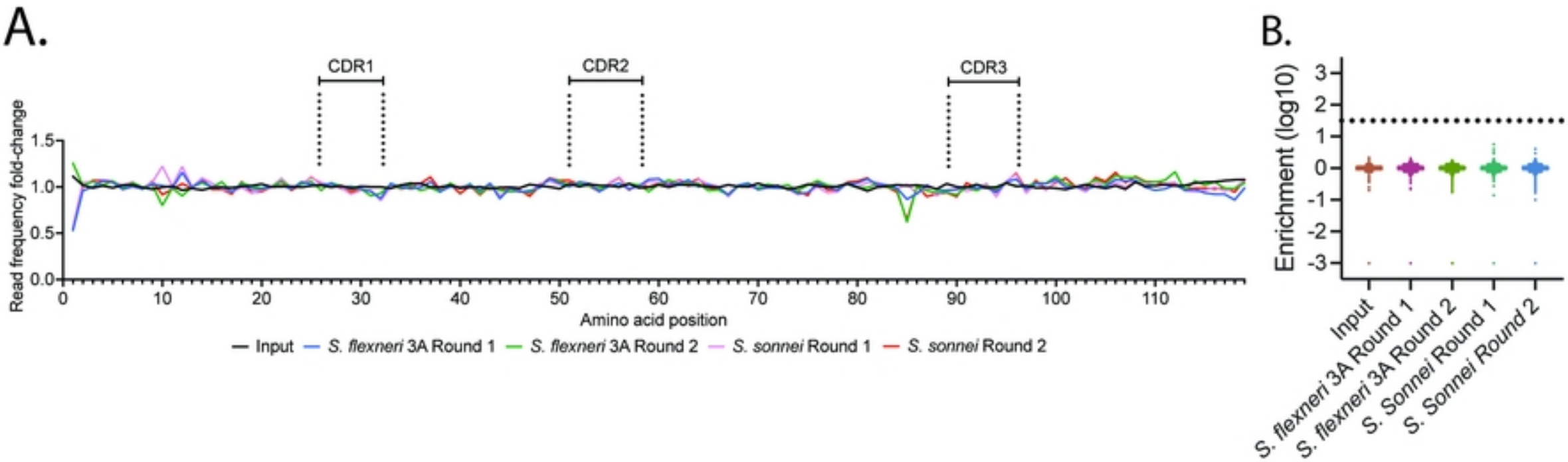
A.
CDR1
CDR2
CDR3
Read frequency fold-change
1.5
1.0
0.5
0.0
0
10
20
30
40
50
60
70
80
90
100
110
Amino acid position
Input
S. flexneri 3A Round 1
S. flexneri 3A Round 2
S. sonnei Round 1
S. sonnei Round 2
B.
Enrichment (log10)
3
2
1
0
-1
-2
-3
Input
S. flexneri 3A Round 1
S. flexneri 3A Round 2
S. Sonnei Round 1
S. Sonnei Round 2

Figure S1

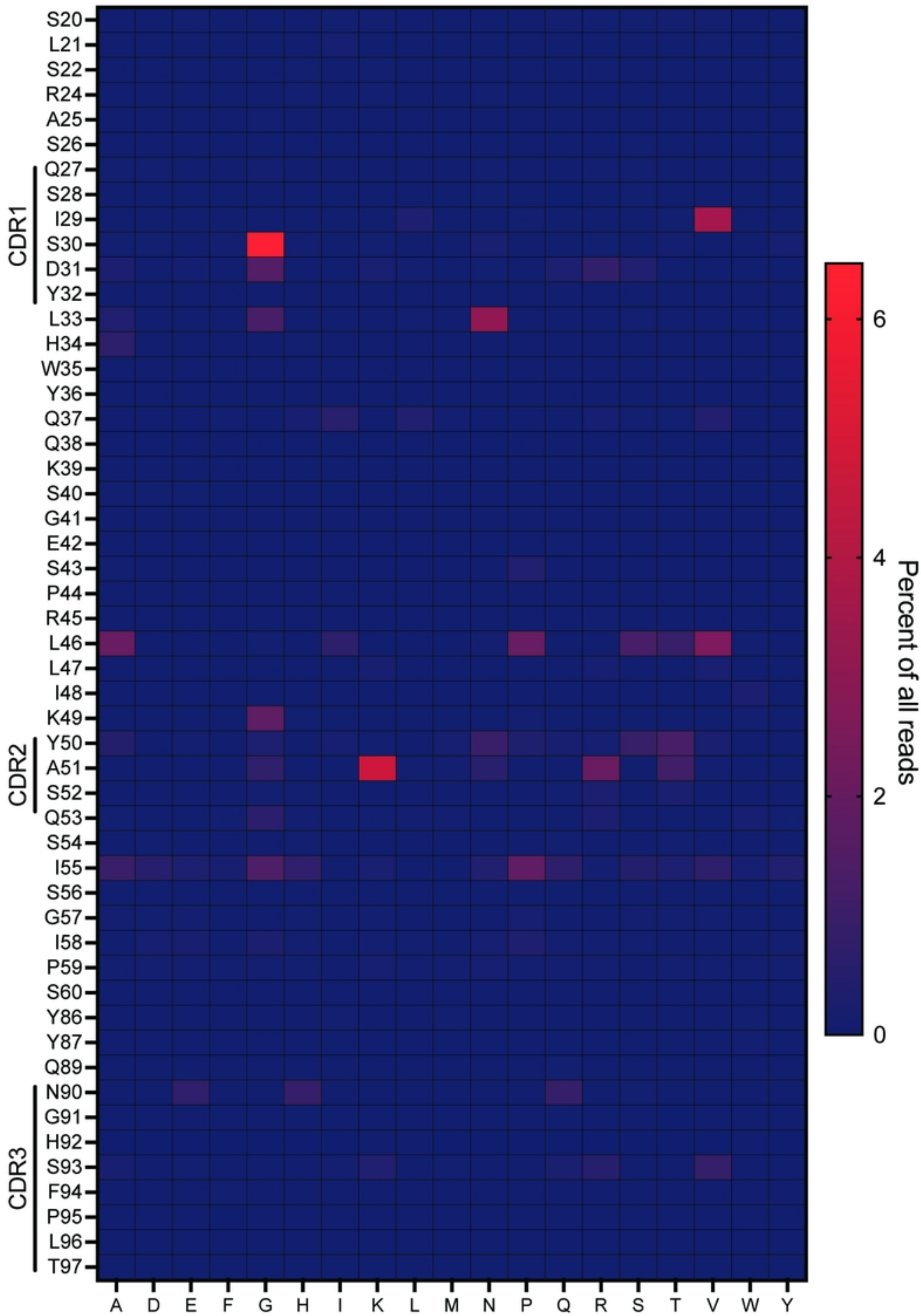
S20
L21
S22
R24
A25
S26
Q27
S28
I29
S30
D31
Y32
L33
H34
W35
Y36
Q37
Q38
K39
S40
G41
E42
S43
P44
R45
L46
L47
I48
K49
Y50
A51
S52
Q53
S54
I55
S56
G57
I58
P59
S60
Y86
Y87
Q89
N90
G91
H92
S93
F94
P95
L96
T97
CDR1
CDR2
CDR3
A D E F G H I K L M N P Q R S T V W Y
6
4
2
0
Percent of all reads

Figure S2

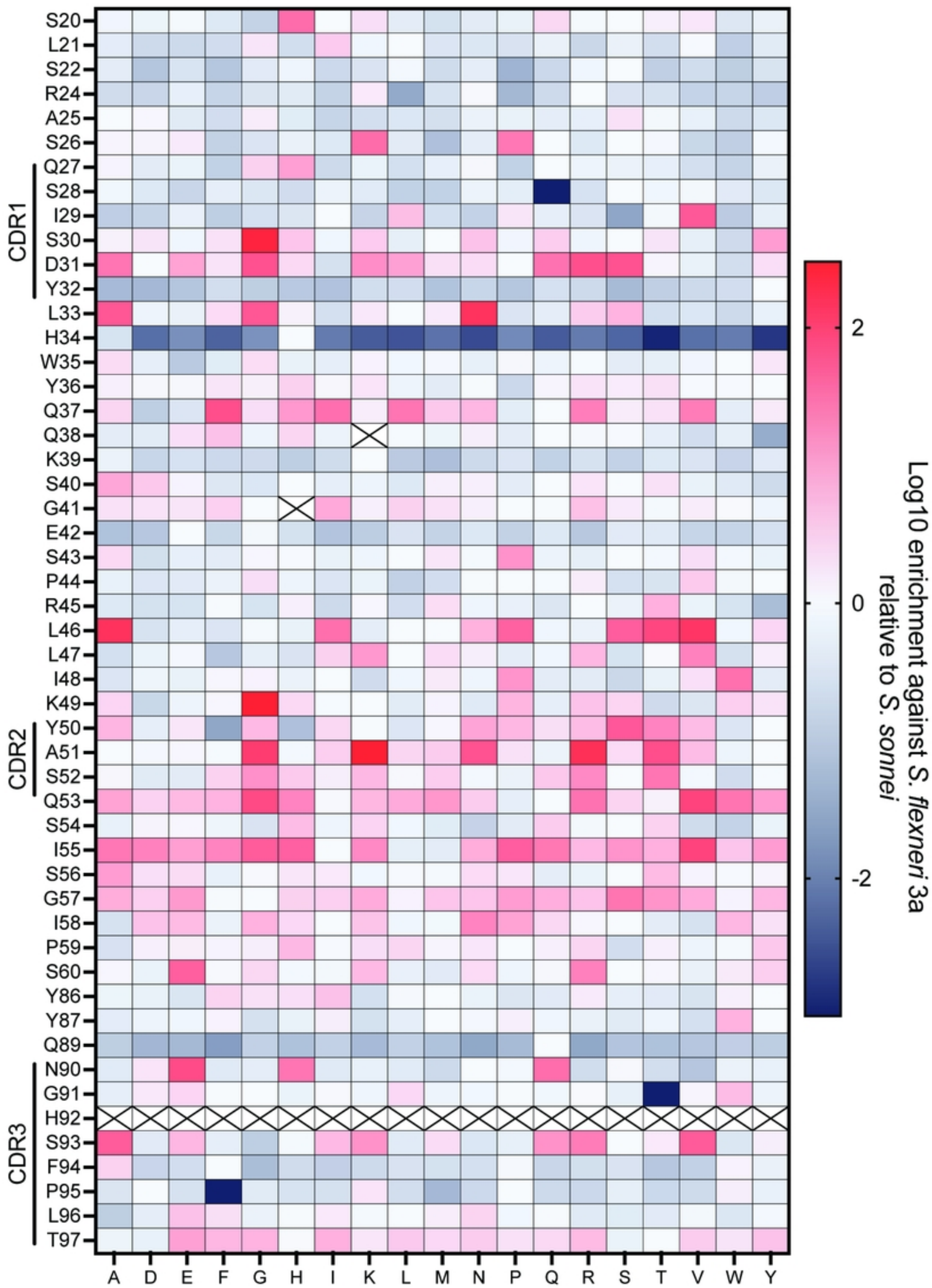
S20
L21
S22
R24
A25
S26
Q27
S28
I29
S30
D31
Y32
L33
H34
W35
Y36
Q37
Q38
K39
S40
G41
E42
S43
P44
R45
L46
L47
I48
K49
Y50
A51
S52
Q53
S54
I55
S56
G57
I58
P59
S60
Y86
Y87
Q89
N90
G91
H92
S93
F94
P95
L96
T97
CDR1
CDR2
CDR3
A D E F G H I K L M N P Q R S T V W Y
2
0
-2
Log10 enrichment against S. flexneri 3a
relative to S. sonnei

Figure S3

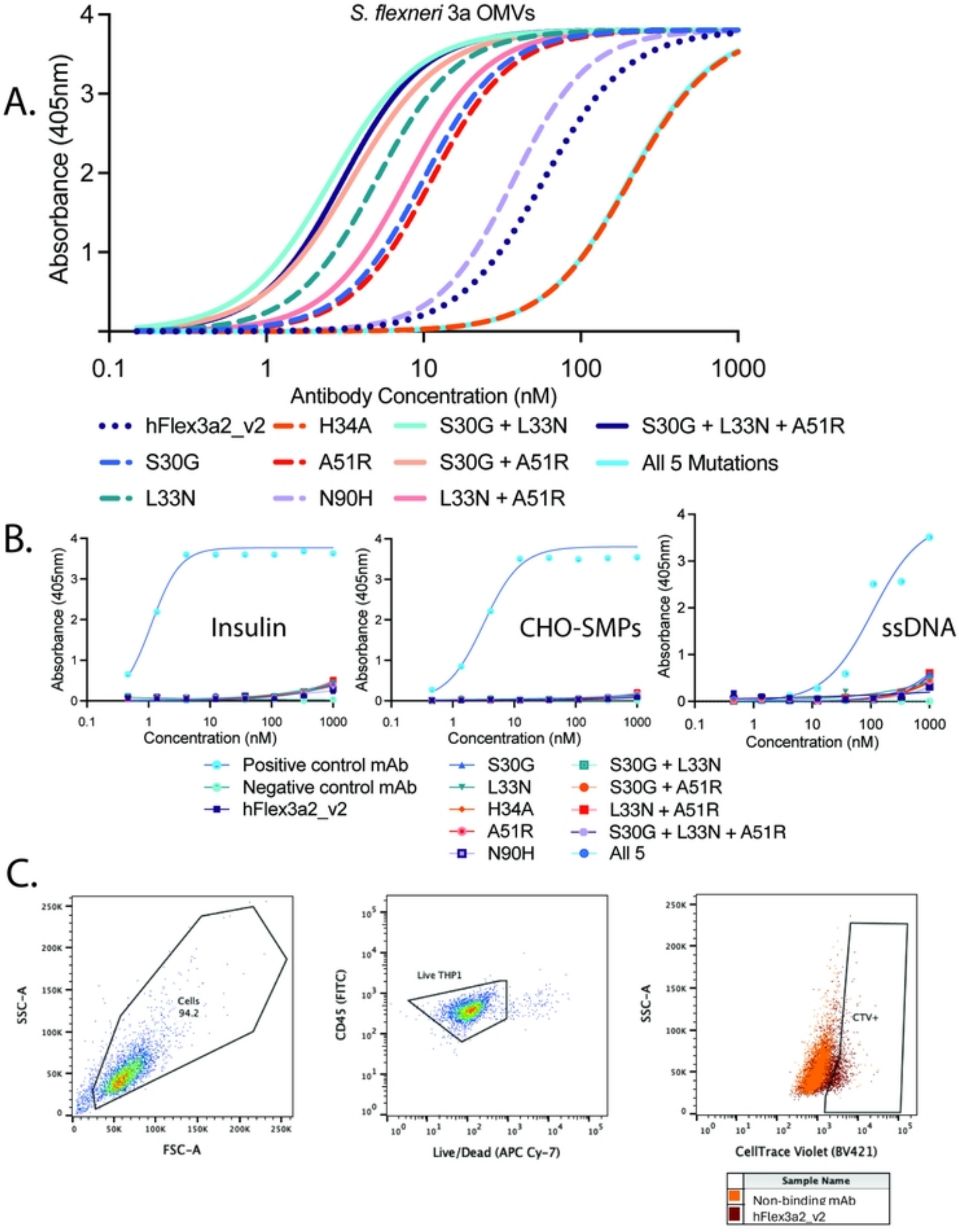
A.
S. flexneri 3a OMVs
Absorbance (405nm)
Antibody Concentration (nM)
hFlex3a2_v2
H34A
S30G + L33N
S30G + L33N + A51R
S30G
A51R
S30G + A51R
All 5 Mutations
L33N
N90H
L33N + A51R
B.
Insulin
CHO-SMPs
ssDNA
Absorbance (405nm)
Concentration (nM)
Positive control mAb
Negative control mAb
hFlex3a2_v2
S30G
L33N
H34A
A51R
N90H
S30G + L33N
S30G + A51R
L33N + A51R
S30G + L33N + A51R
All 5
C.
SSC-A
FSC-A
Cells
94.2
CD45 (FITC)
Live/Dead (APC Cy-7)
Live THP1
CellTrace Violet (BV421)
CTV+
Sample Name
Non-binding mAb
hFlex3a2_v2

Figure S4

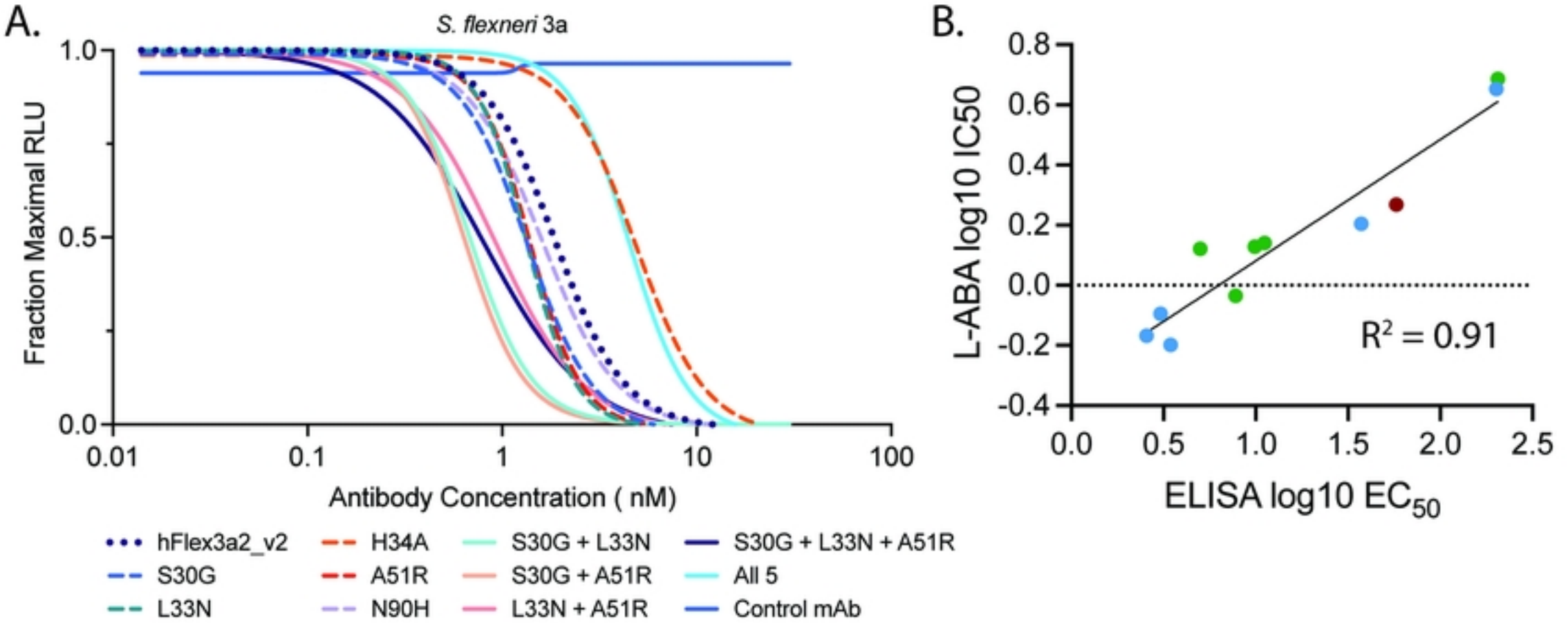
A.
S. flexneri 3a
Fraction Maximal RLU
1.0
0.5
0.0
0.01
0.1
1
10
100
Antibody Concentration (nM)
hFlex3a2_v2
S30G
L33N
H34A
A51R
N90H
S30G + L33N
S30G + A51R
L33N + A51R
S30G + L33N + A51R
All 5
Control mAb
B.
L-ABA log10 IC50
0.8
0.6
0.4
0.2
0.0
-0.2
-0.4
0.0
0.5
1.0
1.5
2.0
2.5
ELISA log10 EC50
R² = 0.91

Figure S5

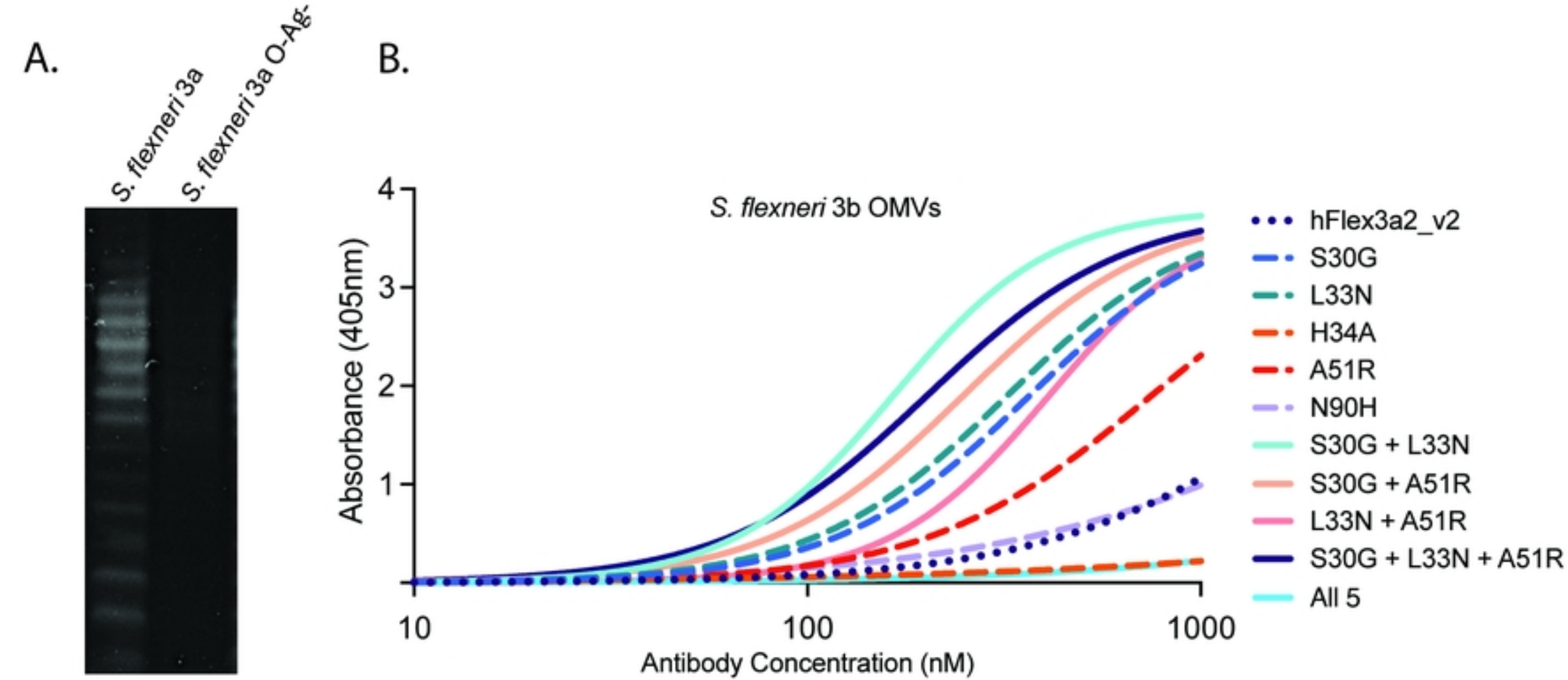
A.
S. flexneri 3a
S. flexneri 3a O-Ag-
B.
S. flexneri 3b OMVs
Absorbance (405nm)
4
3
2
1
10
100
1000
Antibody Concentration (nM)
hFlex3a2_v2
S30G
L33N
H34A
A51R
N90H
S30G + L33N
S30G + A51R
L33N + A51R
S30G + L33N + A51R
All 5

Figure S6

hFlex3a2 protein sequence	
Heavy Chain	QVQLQQSAPELARPGASVKMSCKASGYTFTSYTIHWVKQRPGQGLEWIGYI SPSSGYTEYNQKFKDKTTLTADKSSITAYMQLSSLTSEDSAVYYCARLDNN YVYFDYWGLGTTLTVSS
Light Chain	DIVMTQSPATLSVTPGDRVSLSCRASQSISDYLHWYQQKSHESPRLLIKYAS QSISGIPSRFSGSGSGSDFTLSINSVEPEDVGVYYCQNGHSFPLTFGAGTKLEL K
hFlex3a2_v2 protein sequence	
Heavy Chain	QVQLQQS**G**PELARPGASVKMSCKASGYTFTSYTIHWVKQRPGQGLEWIGYI SPSSGYTEYNQKFKDKTTLTADKSS**S**TAYMQLSSLTSEDSAVYYCARLDNN YVYFDYWGLGTTLTVSS
Light Chain	DIVMTQSPATLSVTPGDRVSLSCRASQSISDYLHWYQQKS**G**ESPRLLIKYAS QSISGIPSRFSGSGSGSDFTLSINSVEPEDVGVYYCQNGHSFPLTFGAGTKLEL K

Underlined residues indicate sites that are different between hFlex3a2 and hFlex3a2_v2

Red residues indicate sites of amino acid changes for affinity matured variants:
S30G, L33N, H34A, A51R, and N90H

Table S1

Table S2. Strains and plasmids used in this study.

Strain or plasmid	Description	Reference/Source
E. coli		
NEB5α	Cloning strain	New England Biolabs
XL1-Blue	Phage library construction	Agilent Technologies
BL21	Protein expression	New England Biolabs
Shigella		
S. flexneri 210059	Serotype 1b	(1)
S. flexneri 2457T	Serotype 2a	WRAIR
S. flexneri CDC 3591-52	Serotype 2b	ATCC 12022
S. flexneri J17B	Serotype 3a	WRAIR
S. flexneri WS-016	Serotype 3b	This study
S. flexneri WS-037	Serotype Y	This study
S. sonnei 53G lvp::kan	LVP stable *S. sonnei*	
S. flexneri J17B *tolR*::kan	tolR knockout, overproduces serotype 3a OMVs	This study
S. flexneri J17B *waaL*::kan	waaL knockout, serotype 3a O-Ag negative strain	This study
S. flexneri r08028 *tolR*::kan	tolR knockout, overproduces serotype 3b OMVs	This study
Human		
HeLa	Virulence assays	ATCC CCL-2
Expi293	Antibody transfection	Thermo Fisher Scientific
THP-1	OPA	ATCC TIB-202
Plasmids		
pACBSR	Gene-gorging mutagenesis vector	(2)
pKD4	Kan resistance casette	(3)
pGEMTeasy	Donor plasmid for gorging	Promega
pET28b (+)	Protein expression vector	Sigma Aldrich
pCOMB3XSS	Phage display vector	(4)

Works Cited:

1. Tansarli GS, Long DR, Waalkes A, Bourassa LA, Libby SJ, Penewit K, Almazan J, Matsumoto J, Bryson-Cahn C, Rietberg K, Dell BM, Hatley NV, Salipante SJ, Fang FC. 2023. Genomic reconstruction and directed interventions in a multidrug-resistant Shigellosis outbreak in Seattle, WA, USA: a genomic surveillance study. Lancet Infect Dis 23:740–750.

2. Herring CD, Glasner JD, Blattner FR. 2003. Gene replacement without selection: regulated suppression of amber mutations in Escherichia coli. Gene 311:153–163.

3. Datsenko KA, Wanner BL. 2000. One-step inactivation of chromosomal genes in Escherichia coli K-12 using PCR products. Proc Natl Acad Sci U S A 97:6640–6645.

4. Andris-Widhopf J, Rader C, Steinberger P, Fuller R, Barbas CF. 2000. Methods for the generation of chicken monoclonal antibody fragments by phage display. J Immunol Methods 242:159–181.

Name	Sequence (5'-3')	Purpose
pKD4F	GTGTAGGCTGGAGCTGCTTC	Amplify Kan cassette
pKD4R	CATATGAATATCCTCCTTAG	Amplify Kan cassette
waaL_downstreamSceIF	TGGCGGCCGCGGGAATTCGATTTAGGGATAACAGGGTAAT TTGGCCGCTGCTCAC	Amplify downstream for waaL mutagenesis
waaL_downstreamR	GAAGCAGCTCCAGCCTACACGTAAAAAATAAAAAAGGCTGC	Amplify downstream for waaL mutagenesis
waaL_upstreamF	CTAAGGAGGATATTCATATGGTCATCTTATCTCCGATG	Amplify upstream for waaL mutagenesis
waaL_upstreamSceIR	GCCGCGAATTCACTAGTGATATAGGGATAACAGGGTAAT GCGATTATGCTATCGCA	Amplify upstream for waaL mutagenesis
tolR_upstreamSceIF	TAGGGATAACAGGGTAATTTGCTTCTGCTTTAACTCGG	Amplify upstream for tolR mutagenesis
tolR_upstreamR	GAAGCAGCTCCAGCCTACACTAAACATCTGCGTTTCCCTTGCTTG	Amplify upstream for tolR mutagenesis
tolR_downstreamF	CTAAGGAGGATATTCATATGCATGGCTTACCCCTTGTTGC	Amplify downstream for tolR mutagenesis
tolR_downstreamSceIR	TAGGGATAACAGGGTAATTCTGGAATCGAACTCTCTCG	Amplify downstream for tolR mutagenesis
phage_library_Amp_F	CTCAGTGGCCCAGGCGGCC	Amplify phage display library for pCOMB3xss
phage_library_Amp_R	CTCAGTGGCCGGCCTGGCC	Amplify phage display library

		for pCOMB3XSS
S30G_F	GAGTATTGGTGACTACTTACA	Clone hFlex3a2_v2 variants
S30G_R	TGTAAGTAGTCACCAATACTC	Clone hFlex3a2_v2 variants
L33N_F	GACTACAATCACTGGTATCA	Clone hFlex3a2_v2 variants
L33N_R	TGATACCAGTGATTGTAGTC	Clone hFlex3a2_v2 variants
H34A_F	GACTACTTAGCGTGGTATCA	Clone hFlex3a2_v2 variants
H34A_R	TGATACCACGCTAAGTAGTC	Clone hFlex3a2_v2 variants
A51R_F	CAAATATCGTTCCCAATCCA	Clone hFlex3a2_v2 variants
A51R_R	TGGATTGGGAACGATATTTG	Clone hFlex3a2_v2 variants
N91H_F	ACTGTCAACATGGTCACAGC	Clone hFlex3a2_v2 variants
N91H_R	GCTGTGACCATGTTGACAGT	Clone hFlex3a2_v2 variants